

Review

Interplay between Light and Functionalized Silk Fibroin and Applications

Fan Hu,^{1,2} Naibo Lin,^{2,*} and X.Y. Liu^{1,2,*}

Silkworm silk has been considered to be a luxurious textile for more than five thousand years. Native silk fibroin (SF) films have excellent (ca. 90%) optical transparency and exhibit fluorescence under UV light. The silk dyeing process is very important and difficult, and methods such as pigmentary coloration and structural coloration have been tested for coloring silk fabrics. To functionalize silk that exhibits fluorescence, the *in vivo* and *in vitro* assembly of functional compounds with SF and the resulting amplification of fluorescence emission are examined. Finally, we discuss the applications of SF materials in basic optical elements, light energy conversion devices, photochemical reactions, sensing, and imaging. This review is expected to provide insight into the interaction between light and silk and to inspire researchers to develop silk materials with a consideration of history, material properties, and future prospects.

INTRODUCTION

Silk is a fine continuous protein fiber produced by spiders or insect larvae. Spiders spin threads of silk to make cocoons for their eggs and webs to catch prey, and such silks have been admired for their extraordinary mechanical properties since ancient times. However, although the application of spiders for silk production is limited because spiders cannot be raised, silk produced by insect larvae such as silkworms is a world-renown fiber. Silkworm silk, which is regarded as “the queen of fibers,” has been widely used in the textile industry for more than five thousand years, and it is the symbol of ancient China’s foreign trade (Service, 2008; Vepari and Kaplan, 2007). A key factor that makes silk fabrics popular in China and throughout the world is their lustrousness, which is due to their special mesoscopic structure and reflective properties. Silk fabrics hold color well, and the Chinese characters 緋 (deep red), 红 (red), and 绿 (green), which incorporate the character 纟 (silk), refer to the colors of silk. The colors of silk fabrics represented status in ancient China; for example, the emperors’ clothes were gold and purple, which were colors ordinary people were not allowed to wear. Four famous brocades representing the historical and cultural heritage of China and the world are Yun, Zhuang, Shu, and Song, which are all famous for their brilliant colors. Five thousand years ago, Chinese people began to develop the techniques for printing and dyeing silk (染纈) to obtain silks of different colors.

With the development of material science, silk is no longer limited to the traditional textile industry, and it is currently regarded as one of the most promising materials of the 21st century. Recently, silk has attracted great interest as high-performance material due to its properties (Place et al., 2009), i.e., excellent optical characters, robust mechanical properties, *in vitro* and *in vivo* biocompatibility, and slow proteolytic biodegradation (Vepari and Kaplan, 2007). Furthermore, although functionalized silk materials exhibit various targetable properties and extraordinary performance, especially in optical applications, few reviews have investigated the development of silk materials for optical applications.

This paper comprehensively reviews the interaction between light and functionalized silk based on silk functionalization approaches and the latest progress in this field. The intrinsic performance of silk materials is firstly evaluated in terms of the transparency of silk fibroin (SF) films, UV absorption, and autofluorescence. The coloring of silk proteins using normal dyeing techniques and bioinspired structural color techniques is also reviewed. In addition to genetic engineering and feeding techniques, the functionalization of SF materials that exhibit fluorescence is highlighted by the incorporation of organic molecules or inorganic nanoparticles into SF materials. Finally, we summarize the use of silk materials for optical applications, such as optical elements, nonlinear optics, light energy conversion, photochemical reactions, UV resistance, photocatalysis, light-assisted synthesis, sensors, and bioimaging. This review is expected to inspire researchers to examine the interaction between light and silk and to develop silk materials with a consideration of history, material properties, and future prospects.

¹Institute of Advanced Materials, East China Jiaotong University, No. 808 Shuanggang East Street, Nanchang 330013, China

²Research Institution for Biomimetics and Soft Matter, Fujian Key Provincial Laboratory for Soft Functional Materials Research, College of Materials, Xiamen University, Shenzhen Research Institute of Xiamen University, 422 Siming South Road, Xiamen 361005, China

*Correspondence: linnaibo@xmu.edu.cn (N.L.), phyluxy@hotmail.com (X.Y.L.)

<https://doi.org/10.1016/j.isci.2020.101035>



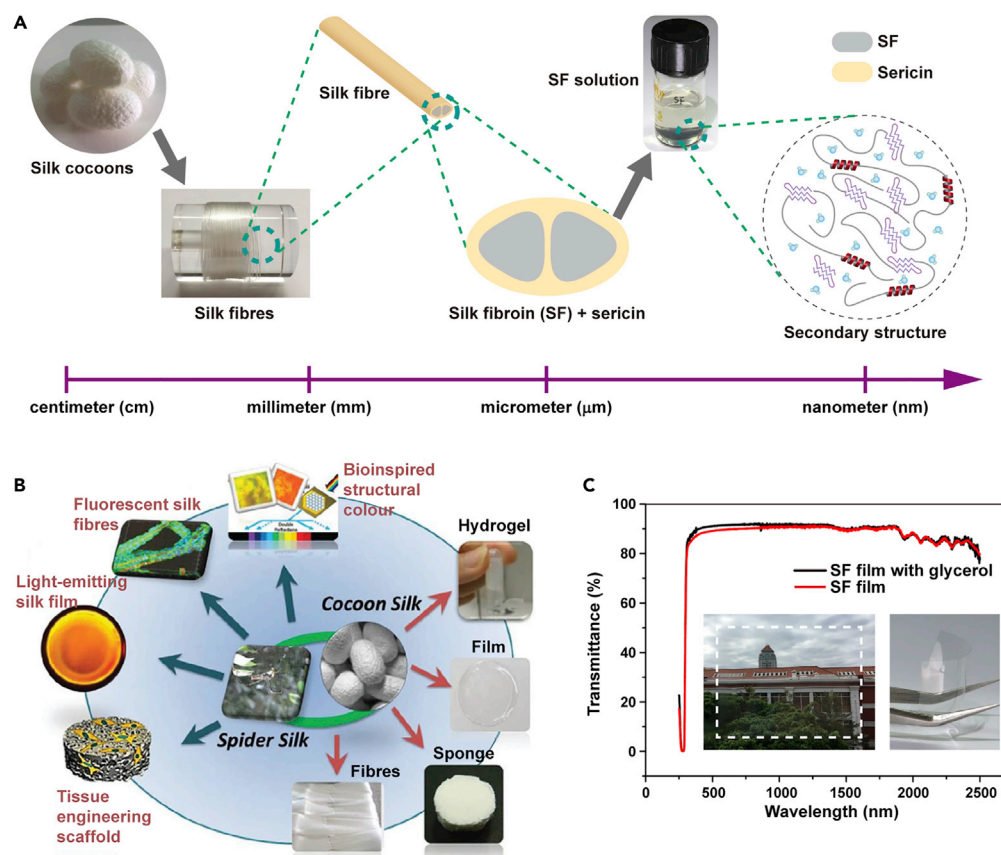


Figure 1. Silk Materials and Regenerated Silk Derivatives

(A) Structure of silk materials based on scale.

(B) Various forms of spider silk and cocoon silk and regenerated silk derivatives, i.e., silk hydrogels, films, sponges, and fibers, applied for bioinspired structural color, fluorescent materials, light-emitting devices, and tissue engineering.

Reprinted with permission from Lin et al., 2015. Copyright 2015, Royal Society of Chemistry.

(C) Transmittance spectra of SF/glycerol film and SF film. Inset: images of a transparent SF film and a curved SF film.

INHERENT OPTICAL PROPERTIES OF SILK FIBROIN MATERIALS

Silkworm silk comes from the silk cocoon that a silkworm spins around itself to build as a natural defense (Figure 1A). A single silk fiber extracted from a *Bombyx mori* cocoon is separated into the sericin coating and the core fibroin filaments. The SF can be dissolved in aqueous solution or organic solvents for further use. SF solution can be processed into various forms of regenerated silk derivatives, i.e., silk films, fibers, hydrogel, and sponges (Figure 1B). SF films are easily prepared from the SF solution by casting the solution onto a substrate and allowing the solvent to evaporate. Notably, as-cast silkworm SF films, which have weak mechanical properties and α -helix-rich structures, have excellent (ca. 90%) optical transparency across the visible and near-infrared range (ca. 280–2500 nm) when prepared under all-aqueous processing (Figure 1C).

SF proteins can exhibit fluorescence without any dyes or markers being employed because they contain amino acids such as tryptophan in sufficiently high concentrations for excitation with a suitable wavelength of UV light. SF can be excited with 280-nm UV light and emit light at approximately 350 nm, but the actual emission wavelength varies based on the polarity of the environment. Furthermore, the fluorescence intensity is not very strong, and the fluorescence of silk under UV light interferes with imaging when cells dyed with blue fluorescence are grown on silk biomaterials. Sudan Black B can quell the autofluorescence of silk and improve the imaging of cells on silk biomaterials (Neo et al., 2015). Native SF can also be prepared as microcapsules that exhibit autofluorescence in the visible range upon near-UV excitation and display a high level of photostability (Shimanovich et al., 2018).

The refractive index and absorption coefficient of SF are investigated. The refractive index is influenced by the residual water content in the silk films and the crystallinity of the SF (but not by the molecular weight of the

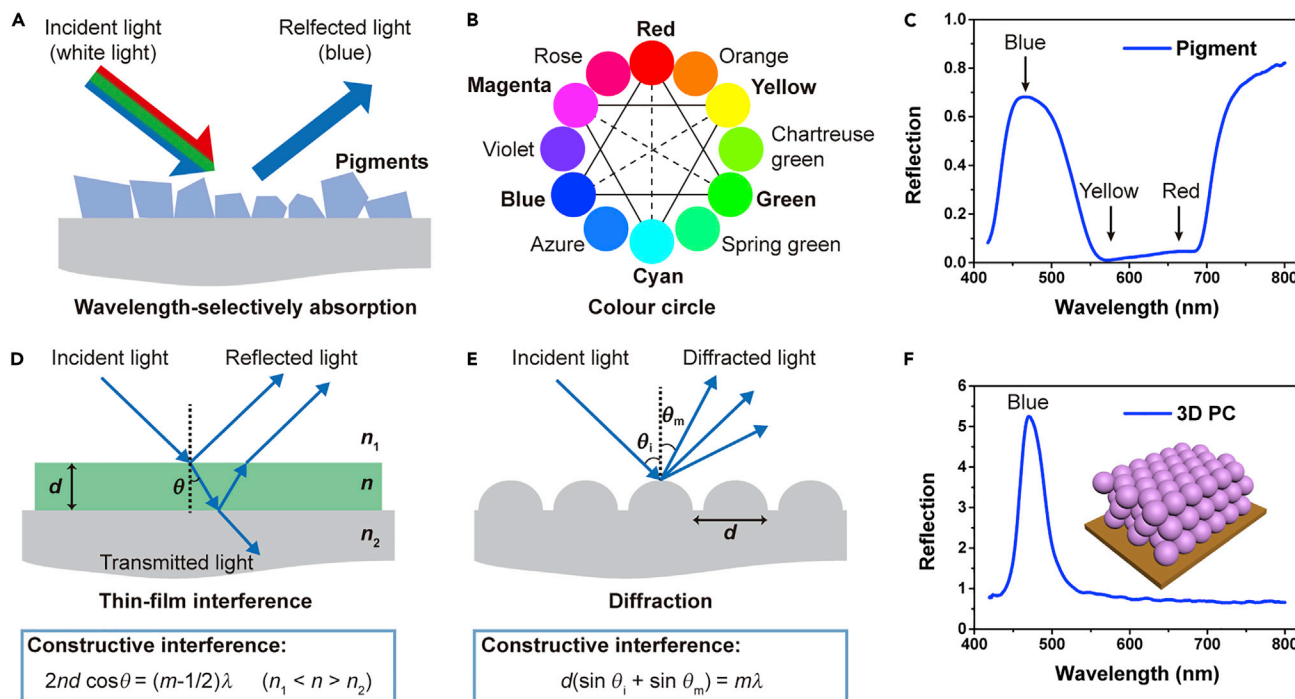


Figure 2. Pigmentary Coloration and Structural Coloration

(A) Schematic of pigmentary coloration from a blue sample. When white light encounters blue pigment, the pigment absorbs red and green light but reflects/scatters blue, creating the appearance of the color blue.

(B) Color circle. Complementary colors are opposite each other.

(C) Measured reflection spectrum of a blue sample.

(D) Schematic of thin-film interference. A thin SF film (green) with a thickness of d is used to coat a glass substrate (gray) in air. Note that n , n_1 , and n_2 are the refractive indices of the thin SF film (ca. 1.54), the upper air medium (ca. 1.00), and the lower glass substrate (ca. 1.50), respectively. The refracted angle in the thin film is θ , the light wavelength in vacuum is λ , and m is an integer.

(E) Schematic of diffraction by a periodically patterned grating. Note that the incident angle is θ_i , the diffracted angle is θ_m , and the grating period is d . The light wavelength in vacuum is λ , and m is an integer.

(F) Measured reflection spectrum of a 3D PC sample consisting of monodispersed colloidal polystyrene (PS) nanospheres packed in a face-centered cubic (FCC) structure. Inset: schematic of the 3D PC structure.

silk). For regenerated silk, $n = 1.554$ at 500 nm, and this value increased to $n = 1.559$ at 500 nm upon crystallization, with an absorption coefficient less than or equal to 10^{-4} for wavelengths longer than 500 nm (Perotto et al., 2017). Upon exposure to γ -irradiation, the refractive index of *Bombyx mori* SF films increases with increasing radiation dosage (Madhukumar et al., 2015). The refractive index of sericin films is slightly higher than that of regenerated SF, suggesting the possibility of using sericin and regenerated SF in combination to produce light guides (Bucciarelli et al., 2018). The birefringence of brown silk fiber (*Antheraea pernyi*) measured by polarized light imaging microscopy is $\Delta n \approx 1.63 \times 10^{-2}$ (with $\sim 2\%$ uncertainty) averaged over the wavelength range $\lambda = 425\text{--}625$ nm (Honda et al., 2018). Moreover, Anderson light localization is observed in *Bombyx mori* silk with quasi-two-dimensional protein nanostructures that have optical window of resonant tunneling in physically closed structures while suppressing most transmission in the visible spectrum and emitting thermal radiation (Choi et al., 2018).

COLORATION OF SILK FIBROIN MATERIALS

Coloration is generally divided into two classes: pigmentary coloration, which is mainly due to the wavelength-selective light absorption of pigments, and structural coloration, which is purely produced by physical means (the interactions between photons and the nano-/microstructure). For example, blue pigment can selectively absorb green and red light and reflect/scatter blue light; the reflected light spectrum creates the appearance of the color blue (Figures 2A–2C). For thin films, multilayers, and diffraction gratings, structural coloration can be simply interpreted by interference and diffraction (Figures 2D and 2E). However, many photonic structures, especially 2D and 3D photonic crystal (PC) and amorphous photonic structures, exhibit complicated optical phenomena resulting from the combination of interference,

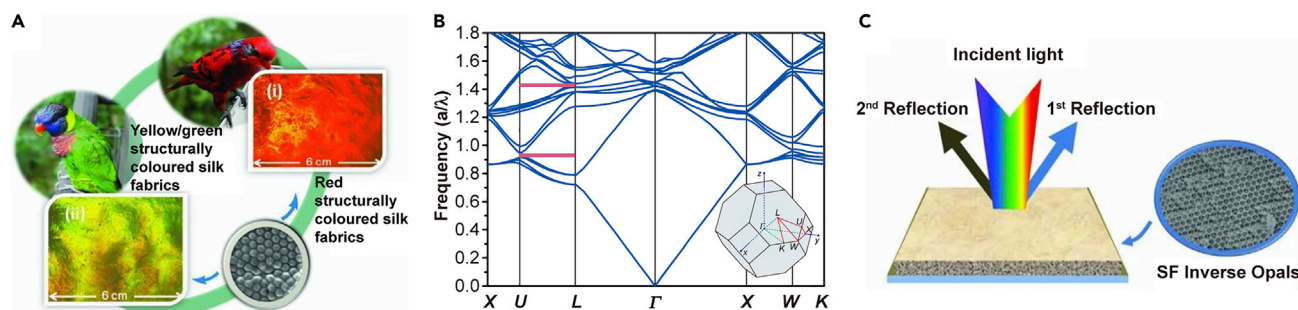


Figure 3. Structural Colors on Silk Fabrics

(A) Biomimetics of structural colors on silk fabrics. Reprinted with permission from Diao et al., 2013. Copyright 2013, John Wiley & Sons, Inc.

(B) Calculated photonic band structure of an SF inverse opal along the high-symmetry directions in the first Brillouin zone. Frequency is in units of a/λ , where a is the lattice constant of the inverse opal and λ is the light wavelength in vacuum. Two partial photonic band gaps (red regions) exist along the L–U direction. Inset: illustration of the first Brillouin zone of the FCC lattice.

(C) Schematic of bistructural colors from an SF inverse opal. Reprinted with permission from Diao et al., 2013. Copyright 2013, John Wiley & Sons, Inc.

diffraction, and scattering. Due to the different coloration mechanisms, structural coloration can achieve bright and highly saturated coloration, herein called “metallic colors” (Figure 2F).

Pigmentary Coloration

For pigmentary coloration, it is feasible to achieve a variety of colorful silk fabrics via dyeing. At present, acid dyes are mainly used to dye silk fabrics; however, the color fastness is not satisfactory. Reactive dyes can covalently bond with silk fibers, and the bonding energy of covalent bonds is much higher than that of hydrogen bonds and van der Waals forces. Therefore, the incorporation of reactive dyes into silk fabrics is expected to fundamentally solve the problem of washing fastness. Heterocyclic monoazo reactive dyes prepared by the diazotization of 3-(4-aminophenyl)-2-phenylquinazolin-4(3H)-one and coupling with a variety of cyanurated coupling components display a variety of color shades with very good depth and uniformity on silk fibers (Parekh and Maheria, 2014).

Natural dyes, such as black carrot and mangrove bark, produce good shades on silk and avoid pollution caused by the production of dyestuff (Punrattanasin et al., 2013). Mordant for dyeing can also be extracted from natural sources. *Emblica officinalis* G. dried fruit tannin gives good color strength, washing fastness, and light fastness in addition to good antibacterial activity (Prabhu et al., 2011). Furthermore, prodiginine extracted from microbial cells of *Zooshikella rubidus* for silk fabric dyeing exhibits grade 1 performance in terms of light fastness and grades 3–5 in terms of color fastness to washing, water, rubbing, perspiration, and dry cleaning, which is similar to the results for other natural dyes (Kim and Choi, 2015). Moreover, by feeding *Bombyx mori* silkworm larvae with a modified feed of mulberry leaves containing a sprayed dye solution, a set of seven different azo dyes can be used to produce intrinsically dyed silk (Nisal et al., 2014). This process significantly reduces the toxic dye effluents that are generated in traditional dyeing processes.

Structural Coloration

Dyeing silk fabrics with structural colors to mimic natural structural color is a well-developed idea, although it has not reached the level of practical application. The color of the PC structure is very sharp and angle dependent, producing vivid and durable structural colors on silk fabrics (Diao et al., 2013). SF inverse opals with different colors are prepared using a simple and inexpensive self-assembly method on silk fabrics (Figure 3), which reflect not only visible light but also UV and near-infrared (NIR) light. The two peaks (λ_1 and λ_2) and the separation between them ($\Delta\lambda$) of the SF inverse opals can be adjusted by changing the lattice constant a , as the midgap frequencies are inversely proportional to a . The midgap wavelength of the first partial photonic bandgap is at $\lambda_1 = 1.429a$, that of the second partial photonic bandgap occurs at $\lambda_2 = 0.685a$, and their separation is $\Delta\lambda = 0.744a$. As the lattice constant a is located in the range $584 \text{ nm} < a < 1022 \text{ nm}$, SF inverse opals with UV/IR or UV/visible reflection peaks are obtained. Such silk fabrics have potential applications in eco-dyeing, UV resistance, thermal insulation, and stealth (Diao et al., 2013).

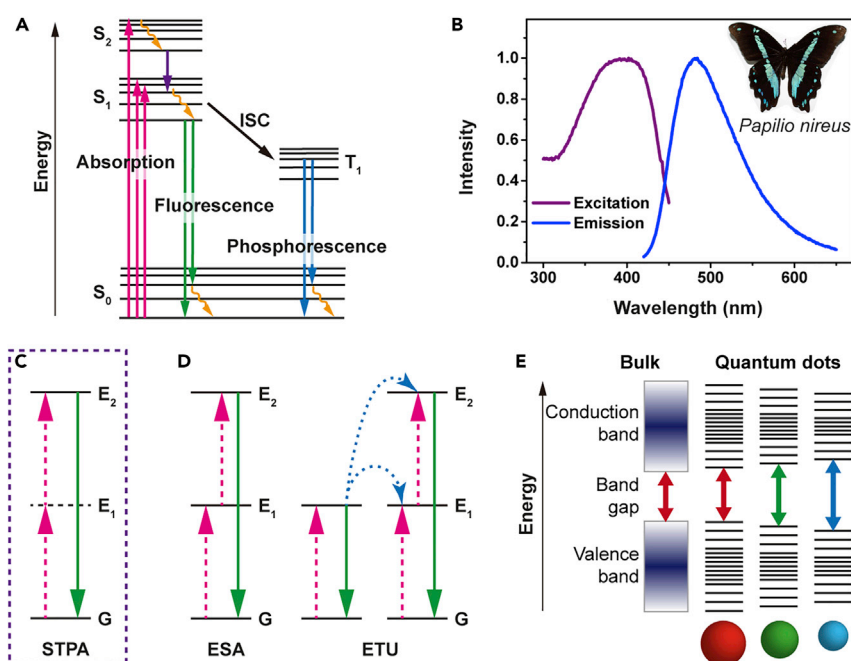


Figure 4. Fluorescence Excitation and Emission

(A) Jablonski diagram of fluorescence emission. An electron is excited after absorbing a low-energy photon (magenta) and immediately relaxes to the ground state by emitting a low-energy photon (green). It can undergo non-radiative relaxation (yellow). The excited electron can also relax via intersystem crossing (ISC) to a triplet state (T_1), which may subsequently relax via phosphorescence (blue) or non-radiative relaxation.

(B) Fluorescence excitation and emission spectra of the blue-green wing scale of the *Papilio nireus* butterfly. Inset: an image of *Papilio nireus*. The wing scales from the colored regions are coated exclusively with fluorescent dyes.

(C) Energy level diagram of the upconversion processes of two-photon dyes: sequential two-photon absorption (STPA). The dashed (magenta) and solid (green) lines represent the photon excitation and emission processes, respectively.

(D) Energy level diagram of the upconversion processes of lanthanide-doped crystals: excited state absorption (ESA) and energy transfer upconversion (ETU). The dashed (magenta), dotted (blue), and solid (green) lines represent the photon excitation, energy conversion, and emission processes, respectively.

(E) Energy level diagram of quantum dots (QDs). The semiconductor band gap is determined by the QD size due to the quantum confinement effect.

FLUORESCENCE EMISSION OF SILK FIBROIN MATERIALS

Fluorescence is the emission of light or other radiation from a substance that has absorbed light or other electromagnetic radiation (Figures 4A and 4B). In this physical process, energy is first absorbed by the substance and then re-radiated at longer wavelengths than the incident light; however, a shorter wavelength can be re-radiated due to multiphoton absorption (Figures 4C and 4D). Fluorescence is a common form of luminescence in nature and practical applications. For fluorescent silk materials, the most appealing is the fact that fluorescence occurs under invisible light (i.e., UV light) but exhibits various striking colors that are visible to humans.

Genetic Modification

Compared with normal proteins with weak fluorescence, fluorescent proteins, such as green fluorescent protein (GFP), yellow fluorescent protein (YFP), and red fluorescent protein (RFP), emit fluorescence with high quantum yields and a wide spectral range covering visible light, and they can be easily imaged by UV microscopes and microspectrophotometers (Agrawal, 1999). Fluorescent silks with green, red, and orange colors have been produced in large quantities from transgenic silkworms obtained using a vector originating from the fibroin H-chain gene and a classical breeding method (Figures 5A–5C). More than 20,000 silkworms were reared to study the suitability of the recombinant silks for making fabrics by harvesting large numbers of cocoons (Iizuka et al., 2013). The silkworm genome was targeted by a targeting vector to construct a transgenic silkworm that spins silk with antibacterial properties and fluorescence (Li et al., 2015). The targeting vector consists of a fusion gene of GFP and the

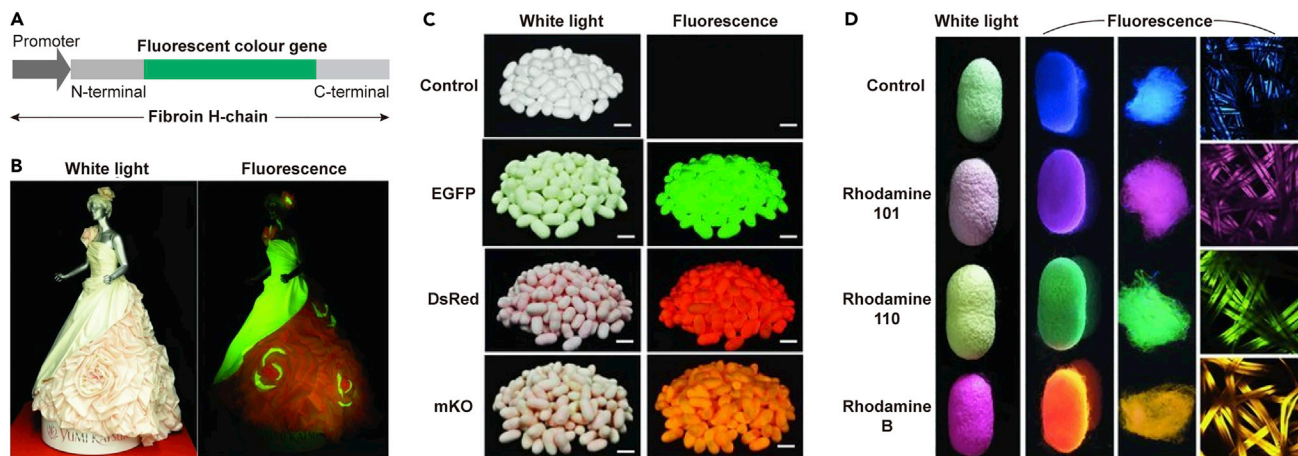


Figure 5. Multi-Colored Fluorescent Silk

(A) Vector structure of the fluorescent color gene encoding (green) flanked by fibroin H-chain N-terminal and C-terminal regions driven by fibroin H-chain promoter (Iizuka et al., 2013).

(B and C) (B) Images of a wedding dress produced by the colored fluorescent silks. (C) Images of colored fluorescent cocoons produced by transgenic silkworms. The image in the left column was taken under white light, whereas that in the right was taken through a yellow filter under blue irradiation. Reprinted with permission from Iizuka et al., 2013. Copyright 2013, John Wiley & Sons, Inc. Scaling bars indicate 2 cm.

(D) Images of colored fluorescent cocoons and fibers produced by normal silkworms (as control) and silkworms fed various fluorescent dyes including rhodamine 101, rhodamine 110, and rhodamine (B). The images in the first row were taken under white light, whereas the other three rows were taken under UV irradiation. Reprinted with permission from Tansil et al., 2011. Copyright 2011, John Wiley & Sons, Inc.

antimicrobial peptide cecropin gene *cec* flanked by pieces of the 5' and 3' sequences of the fibroin L-chain gene *fib-L* and a negative selection *DsRed* marker gene driven by the baculovirus immediate-early gene 1 (i.e., -1) promoter.

The shortcomings of transgenic engineering include high cost, low production efficiency, and high complexity. In most cases, transgenic silkworms are not able to spin silk (Zhang et al., 1999). In addition, the narrow excitation spectra of GFP and other fluorescent proteins limit the selection of excitation light, and the transgenic fluorescent silk fibers are mechanically weaker than the control.

Alternatively, the hybridization technique in genetics can be applied to address similar issues. Because the sex of the silkworm can affect the fluorescence colors of the cocoon, the sex of the Chinese silkworm Dong 34 could be identified based on its fluorescent cocoon colors (Hu et al., 2012). Using systematic segregation and cross-breeding, a pair of silkworm varieties, called "Yingguang" × "Chunyu", was bred. The female silkworm cocoon is white, whereas the male silkworm cocoon is fluorescent yellow under blue UV light. Due to the easy identification of sex by the fluorescence of the silkworms, females can be selected to enable the properties of silkworm silk, such as the fluorescence and mechanical properties, to be refined.

In Vivo Functionalization

Compared with other methods such as dyeing, environmentally friendly feeding methods avoid the discharge of dye waste and the degradation of the mechanical performance of silk fibers during chemical, biological, and heat treatments. In nature, silkworms can be fed foods containing fluorescent pigments, such as flavonoids and their analogues, and these pigments then appear in the cocoons. For example, bamboo-colored cocoons contain seven pigments, and green cocoons contain nine fluorescent pigments, including five flavonoid pigments and four flavonoid analogues. From a physiological point of view, fluorescent dyes, such as flavonoids, are transferred from the midgut to the blood under the control of Green a (*Ga*) genes and from the blood to the silk glands under the control of Green b (*Gb*) genes (Daimon et al., 2010). The dominant genes *Ga* and *Gb* govern the transport of green flavonoids. The Green c (*Gc*) gene can also transfer flavonoids from the midgut to the blood and from the blood to the silk glands via hemolymph, and in addition to *Ga* and *Gb*, it also controls the transport of other flavonoids.

Among feeding methods, a feasible and cost-effective green feeding approach was developed to produce fluorescent silk materials in which the silkworm directly spins a fluorescent silk cocoon after being fed a modified diet. Recently, intrinsically colored and luminescent silks were produced *in vivo* through the direct

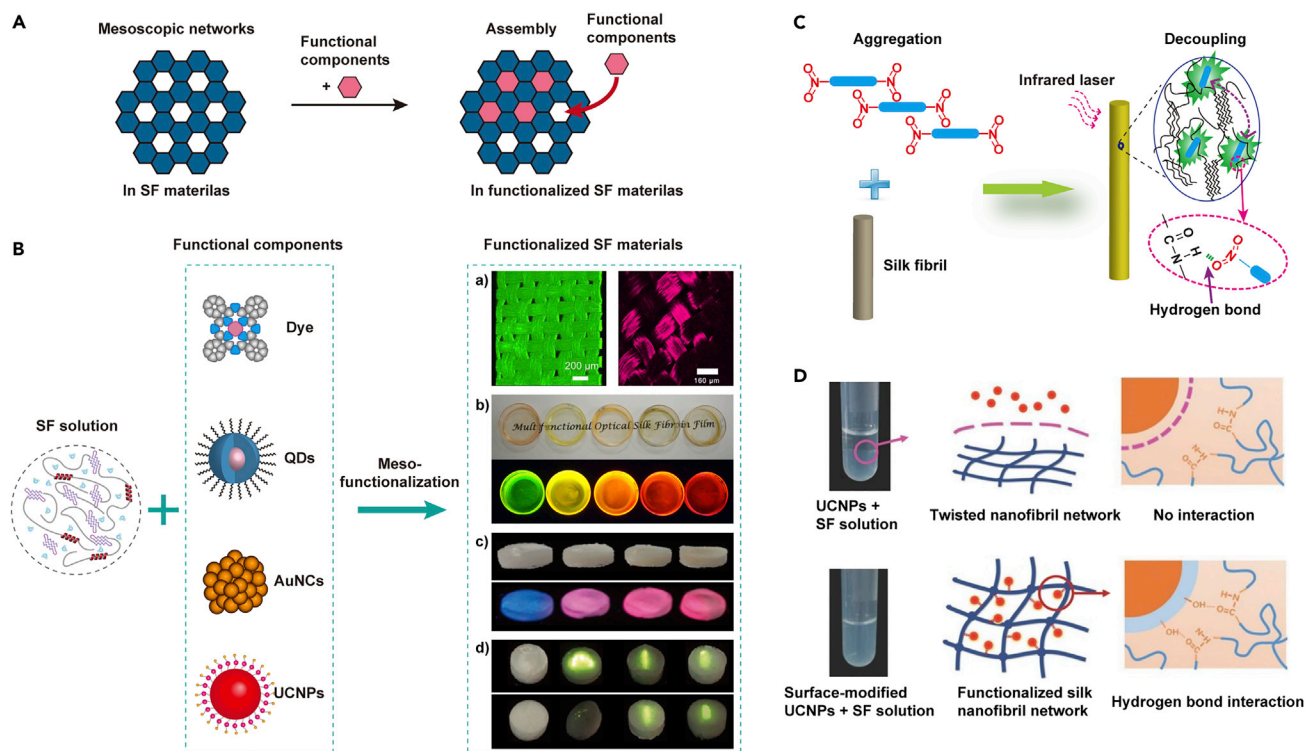


Figure 6. Examples of Meso-functionalization of SF Materials

(A) Schematic illustration of the mesoscopic material assembly (MMA) mechanism.

(B) Illustrations of the silk functionalization process with dye, QDs, Au nanoclusters (AuNCs), and UCNPs.

(a) Two-photon fluorescence (TPF) microscope image of two-photon fluorescent-woven scaffolds. (Left) Reprinted with permission from Lin et al., 2012. Copyright 2012, John Wiley & Sons, Inc. (Right) Reprinted with permission from Lin et al., 2014. Copyright 2014, The Royal Society of Chemistry. Scaling bars indicate 200 μm (left) and 160 μm (right), respectively.

(b) Images of CdTe QDs/SF nanocomposite films (with different QD sizes) under ambient light and under UV light. Reprinted with permission from Lin et al., 2015. Copyright 2015, John Wiley & Sons, Inc.

(c) Images of BSA-AuNCs/silk scaffolds under white light and under UV light. The BSA-AuNCs contents for samples from left to right were 0% (neat silk), 10%, 20%, and 30%. Reprinted with permission from Lin et al., 2016. Copyright 2016, John Wiley & Sons, Inc.

(d) Images of both sides of UCNP-functionalized SF scaffolds under a 980-nm laser. The scaffolds were functionalized by (1) nothing (neat silk), NaYF₄:Yb³⁺/Er³⁺ nanoparticles coated with (2) oleic acid (UCNPs@OA), (3) silica (UCNPs@SiO₂), and (4) polyethylene glycol (UCNPs@PEG). Reprinted with permission from Song et al., 2017. Copyright 2017, John Wiley & Sons, Inc.

(C) Proposed model for the silk fibril decoupling effect by the molecular recognition of organic molecules. Reprinted with permission from Lin et al., 2012. Copyright 2012, John Wiley & Sons, Inc.

(D) Schematic illustration of the functionalization of SF materials by UCNPs via MMA. Reprinted with permission from Song et al., 2017. Copyright 2017, John Wiley & Sons, Inc.

uptake of dye molecules by silkworms (Figure 5D) (Tansil et al., 2011). Furthermore, highly fluorescent organic dyes are taken up *in vivo* by SF and further fabricated based on the feeding method into solutions, fibers, and films that exhibit lasing properties (Cavallini et al., 2015). In addition to dyes, metal nanoparticles/clusters or quantum dots (QDs) are also being added into the diet formulations. The *in vivo* uptake of fluorescent compounds into SF is a green method for the production of colored silk because it avoids the water pollution and resource waste associated with the dyeing process.

In Vitro Functionalization

In vivo assembly has obvious advantages, as discussed earlier; however, the productivity of dye assembly to SF is quite low because most of the dye was removed from the body via feces. Based on mesoscopic material assembly (MMA) (Figures 6A and 6B), a series of two-photon fluorescent organic molecules with/without functional groups, such as 8NF (Lin et al., 2012), 8MF, NF, and MF (Lin et al., 2014), were designed and prepared. All molecules exhibited high fluorescence efficiency in solvent compared with their counterparts in solid form due to the large π conjugation structure obtained by side-by-side molecular stacking. According to molecular recognition, the molecules with

functional nitro groups, 4NF, 8NF, and NF, can interact with the polar groups through strong hydrogen bonds, such as those involving amide and hydroxyl groups in the SF molecules (Figure 6C). As a result, π -stacking is almost eliminated, and the fluorescence efficiency (quantum yield) is highly improved. The molecules with methyl groups instead of nitro groups, 8MF and MF, form no hydrogen bonding interactions and demonstrate no molecular recognition or de-aggregating effect in silk materials, which further supports the existence of the MMA mechanism.

QDs are very small semiconductor nanoparticles with sizes of several nanometres that exhibit obvious quantum effects, and their optoelectronic properties change as a function of both size and shape (Figure 4E). Many types of QDs emit light of specific frequencies if electricity or excitation light is applied to them, and because these frequencies can be precisely tuned by changing the dot size, shape, and material, there are many applications for QDs. The fabrication of bio-hybrid silk films is demonstrated by applying MMA. QDs can be fixed to amide groups in SF films by $-\text{COO}-$ groups functionalized on the QD surface (Lin et al., 2014a). Hydrogen bond molecular recognition between the amide groups of SF and the $-\text{COO}-$ groups on QDs leads to the uniform distribution of QDs in SF materials. The MMA of QDs with silk films has unique advantages, including simple preparation, tuneable white-light emission, easy manipulation, and low fabrication costs, which make it a promising candidate for multicomponent optodevices. White-light-emitting QD silk hybrid films are obtained by the MMA of blue luminescent ZnSe (5.2 nm) and yellow luminescent CdTe (4.1 nm) QDs in a molar ratio of 30:1. Moreover, layer-by-layer-based electrostatic interactions produce silks with bright fluorescence from green to NIR by changing the QD size, which enables the fluorescence to penetrate an opaque pig skin ~ 3.5 mm in thickness (Chu and Liu, 2008). Silk films assembled with CdTe quantum dots can be quenched by hydrogen peroxide (H_2O_2) at concentrations above 0.3×10^{-3} M, indicating that QD-incorporated silk films can be used as optical sensors to achieve oxidation potential in solution (Tsao et al., 2015).

Tens of metal atoms gather in metal nanoclusters with diameters of several nanometres, and these clusters have attractive electronic, optical, and chemical properties compared with nanoparticles with sizes greater than 10 nm. Silk fibers are chemically coated with luminescent gold nanoclusters through the redox reaction between the protein-based silk and an Au salt precursor, which possesses a relatively long wavelength emission, high quantum yields, a long fluorescent lifetime, and photostability (Cohen-Karni et al., 2012; Zhang et al., 2015).

Upconversion nanoparticles (UCNPs) can emit high-energy light under the excitation of low-energy NIR light. Under the guidance of MMA, the surfaces of UCNPs consisting of sodium yttrium fluoride (NaYF_4) codoped with $\text{Yb}^{3+}/\text{Er}^{3+}$ are modified by the hydroxyl groups ($-\text{OH}$) from SiO_2 or polyethylene glycol (PEG) coating layers, which can interact with the carbonyl groups ($\text{C}=\text{O}$) in SF. As shown in Figure 6D, untreated UCNPs could not be successfully incorporated into the SF, whereas surface-modified UCNPs could be incorporated into the SF via the hydrogen bond interaction between the hydroxyl group ($-\text{OH}$) of surface-modified UCNPs and the carbonyl group ($\text{C}=\text{O}$) of SF. As a result, UCNPs can evenly functionalize into SF materials (Song et al., 2017). SF hybrid films assembled with $\text{YVO}_4:\text{Eu}^{3+}$ nanoparticles at low concentration (<5 wt %) are also reported and have exhibited high-quality optical red emission (da Silva et al., 2017). Europium ions are assembled in an SF matrix, and the *Bombyx mori* SF bears aromatic amino acids, such as tyrosine (Tyr) and tryptophan (Trp), that can function as fluorescent probes. The energy of the Trp triplet state allows efficient energy transfer from Trp to the Tb^{3+} ion (Pugina et al., 2019). The MMA method shows the efficient and uniform integration of the luminescent compounds with SF materials, and it is not limited to the above functional materials.

Fluorescence Emission Enhancement by Silk Collimators

Fluorescent silk materials, as a typical class of flexible materials, have attracted significant attention for fabric production, flexible/implantable electronics, and biomedical applications. A simple strategy that controls the mesoscale structures and architectures of soft materials is demonstrated to achieve amplified fluorescence emission due to the collimation effect of silk photonic crystals (PCs) (Hu et al., 2019). As shown in Figures 7A and 7B, the fluorescence emission of SF films increases linearly with the number of layers of the PC structure (0, 5, 15 and 20), and the fluorescence emission is amplified by 40 times with 20 layers. The emission peak ($\lambda_{\text{em}} \approx 553$ nm) does not overlap with the reflection peak of the silk photonic crystals ($\lambda_{\text{PC}} \approx 885$ nm). Moreover, after optimizing the correlation between the photonic band gap (PBG) and fluorescent emission, 10-layer rhodamine 6G (R6G)-doped silk PCs increase the self-fluorescence emission by 50 times (Figure 7C).

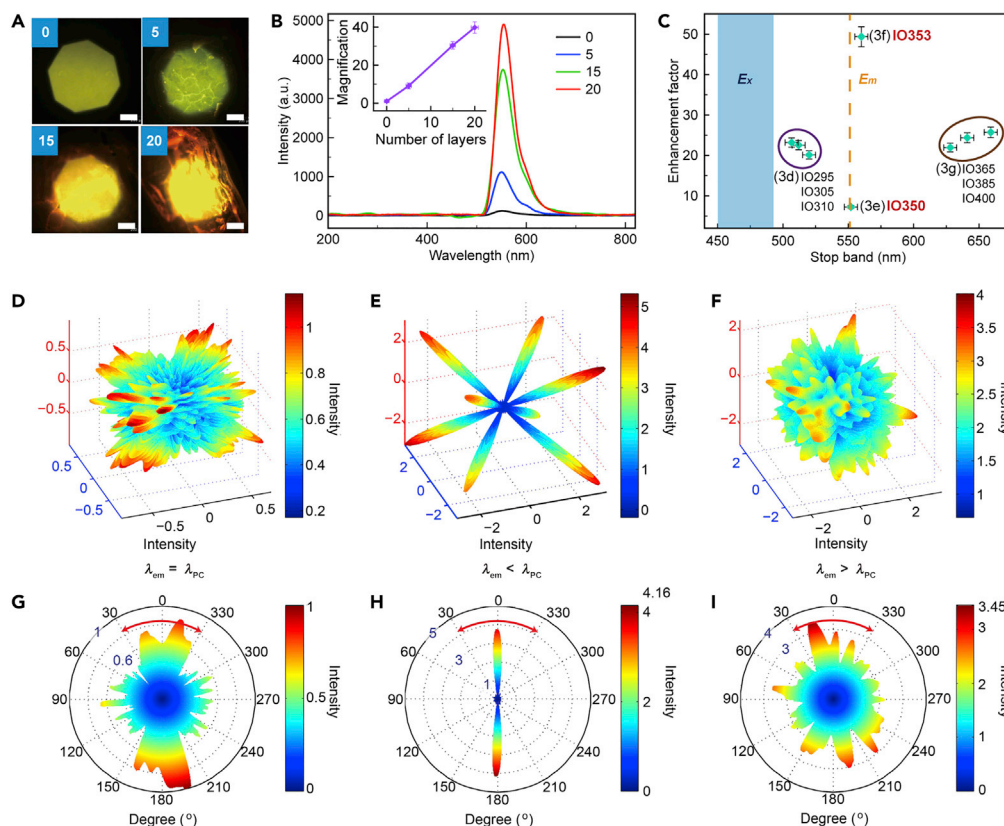


Figure 7. Fluorescence Emission Adjusted by Silk PCs

(A–I) (A) Fluorescence microscopy images of the control (0 layer) and PC films with 5 layers, 15 layers, and 20 layers; scale bar: 500 μm . (B) Fluorescence spectra of R6G-doped silk PCs and the control (e.g., λ : 450–490 nm; E_m , λ : 553 nm). Inset: the amplification of the fluorescence intensity increases as the number of layers of the inverse opal structure increases. (C) Comparison of the fluorescence intensity of silk PCs with different stop bands. (D–I) FDTD simulation of fluorescence emission in different silk PCs. The light emits at the wavelength of λ_{em} , and the wavelength corresponding to the PBG structure is λ_{PC} . (D–F) 3D FDTD simulation of fluorescence emission when (D) $\lambda_{em} = \lambda_{PC}$, (E) $\lambda_{em} < \lambda_{PC}$, and (F) $\lambda_{em} > \lambda_{PC}$. (G–I) 2D vertical sections of FDTD simulations of fluorescence emission when (G) $\lambda_{em} = \lambda_{PC}$, (H) $\lambda_{em} < \lambda_{PC}$, and (I) $\lambda_{em} > \lambda_{PC}$. Reprinted with permission from Hu et al., 2019. Copyright 2019, John Wiley & Sons, Inc.

The effect leading to optimal fluorescence enhancement is illustrated by the finite-difference time-domain (FDTD) simulations in Figures 7D–7I. Briefly, when $\lambda_{em} = \lambda_{PC}$ (Figures 7D and 7G), the fluorescence emission along the $\langle 111 \rangle$ directions of the silk PCs is blocked, and much less fluorescence emission is detected at $\theta \approx 0^\circ$; when $\lambda_{em} < \lambda_{PC}$ (Figures 7E and 7H), due to the low state intensity at the band edge, the fluorescence emission is enhanced at the blue band side of the PCs at $\theta \approx 0^\circ$, which is referred to as the self-collimation effect of fluorescence emission from silk PCs; when $\lambda_{em} > \lambda_{PC}$ (Figures 7F and 7I) the emitted light undergoes internal diffraction at higher angles, and no enhancement is observed.

NONLINEAR OPTICS OF SILK FIBROIN MATERIALS

As an important area in the field of optical physics, the study of the nonlinear optics of silks offers insight into the interaction of intense light with silk materials, including fundamental issues and applications. The multiphoton absorption of SF at 810 nm is determined using the open-aperture Z-scan method, and the increase in the concentration of SF solution results in a linear increase in the three-photon coefficient. The three-photon absorption cross-section is dependent on the molecular weights, and the cross-section was found to increase exponentially with increasing molecular weight (Applegate et al., 2013). SF can also exhibit higher nonlinear optical properties by doping functional materials. A blue-emitting stilbene-doped silk film was spin-coated onto a 1D distributed feedback grating to obtain an organic lasing, whose threshold is lower than that of organic distributed feedback grating lasers based on the same active dye (Toffanin et al., 2012).

Moreover, the solidified silk film possesses extremely large third-order susceptibilities (ca. 10^{-9} esu) in a wide NIR spectral region. The nonlinearity of silk protein can be substantially enhanced by inducing stronger molecular interactions from van der Waals forces and hydrogen bonding (Lee et al., 2016). In the research on the molecular structure of spider silk, the second harmonic generation signal correlates with the existence of the protein β -sheets of dragline, and the β -sheet has a nonlinear response that depends on the direction of the incident electric field (Zhao et al., 2017).

The study of the nonlinear effect of silks has implications for a wide range of applications. A physically transient organic distributed feedback laser was fabricated using optically activated silk bio-ink with sodium fluorescein by spin-coating on a large area 1D fused silica grating (Figures 8A and 8B), and it showed single-mode lasing at a wavelength of 555 nm and a threshold of 13.6 mJ cm^{-2} . The threshold and the differential external quantum efficiency remained steady under repeated washing and recoating (Jung et al., 2016). Furthermore, rhodamine B-doped SF nanofibrous scaffolds with light amplification were fabricated and modulated through the control of the alignment or directionality of SF nanofibres using an electrospinning procedure (Figures 8C and 8D). The scaffolds act as a diffusive random lasing system whose lasing features are strongly related to the structural and mechanical properties of the scaffolds (Kim et al., 2017).

Nonlinear multiphoton interactions of spider silk with few-cycle femtosecond pulses allow for the processing and heterostructuring of the material in ambient air (Figures 8E and 8F). There are two qualitatively different responses, i.e., bulging by multiphoton absorption and plasma-assisted ablation, for low- and high-peak intensities, respectively. Plasma ablation allows us to make localized nanocuts, microrods, nanotips, and periodic patterns with minimal damage when preserving the molecular structure, whereas bulging regime facilitates the confined bending and microwelding of silk with materials such as metal, glass, and Kevlar with strengths comparable to pristine silk (Sidhu et al., 2017).

OPTICAL APPLICATIONS

Optical Elements of Silk Fibroin Materials

Optical elements, which are the basic components of an optical system, are used in imaging applications, such as lenses, prisms, and mirrors. In addition, some play special roles in optical systems, such as spectroscopy, image transmission, and filtering (Ling et al., 2016). For example, the assembly of silver nanoplates to silk film under the same preparation conditions resulted in a hybrid silk with a highly reflective, mirror-like character (Kharlampieva et al., 2010). Titanatenano sheets are also assembled with SF to fabricate tuneable nanocomposites with high refractive indices (Perotto et al., 2015).

Silk Micropatterns

The fabrication of silk materials with microstructures, such as 3D PCs, microlenses, and optical arrays, is a biocompatible method that provides unique opportunities for structurally colored biodegradable materials in microscale implantable biosensing and targeted therapeutics applications (MacLeod and Rosei, 2013; Palermo et al., 2017). A simple soft lithography-based casting technique is used to fabricate SF materials with intricate 2D or 3D nano- or micropatterns (Figure 9A), which enables the fabrication of (at least) sub-30-nm transverse features in SF films from an aqueous silk solution for application in biomedical optics (Perry et al., 2008). These films are of great consequence for use in a variety of studies. Notably, silk sericin can be used as a photoresist for the direct and rapid formation of precise protein microstructures in two and three dimensions with line widths as low as $1 \mu\text{m}$ on a variety of substrates (Figures 9B and 9C). Silk-based microstructures using photolithographic fabrication can provide structural iridescence and guide cell adhesion with precise spatial control (Kurland et al., 2014).

Moreover, the rapid nanoimprinting of SF films at ambient humidity was realized by depositing a small amount of water ($1 \mu\text{L}$) on the film to locally decrease the glass-transition temperature before pressing on the master pattern. The imprinted films are quite stable and last years after exposure to methanol to eliminate water solubility. A self-sensing optofluidic device was constructed to demonstrate that the soft micro- and nanopatterned silk materials are increasingly useful for various optical, mechanical, electronic, microfluidic, and optofluidic devices (Amsden et al., 2010). Doping ease and the ability to readily nanoimprint silk films offer the possibility to rapidly prototype photonic devices that couple optical functions with embedded material properties. By imprinting fluorescent silk films with periodic nanoscale lattices matched to the emission spectra of the doping fluorophores, it is possible to selectively enhance the emission from the film (Mondia et al., 2010).

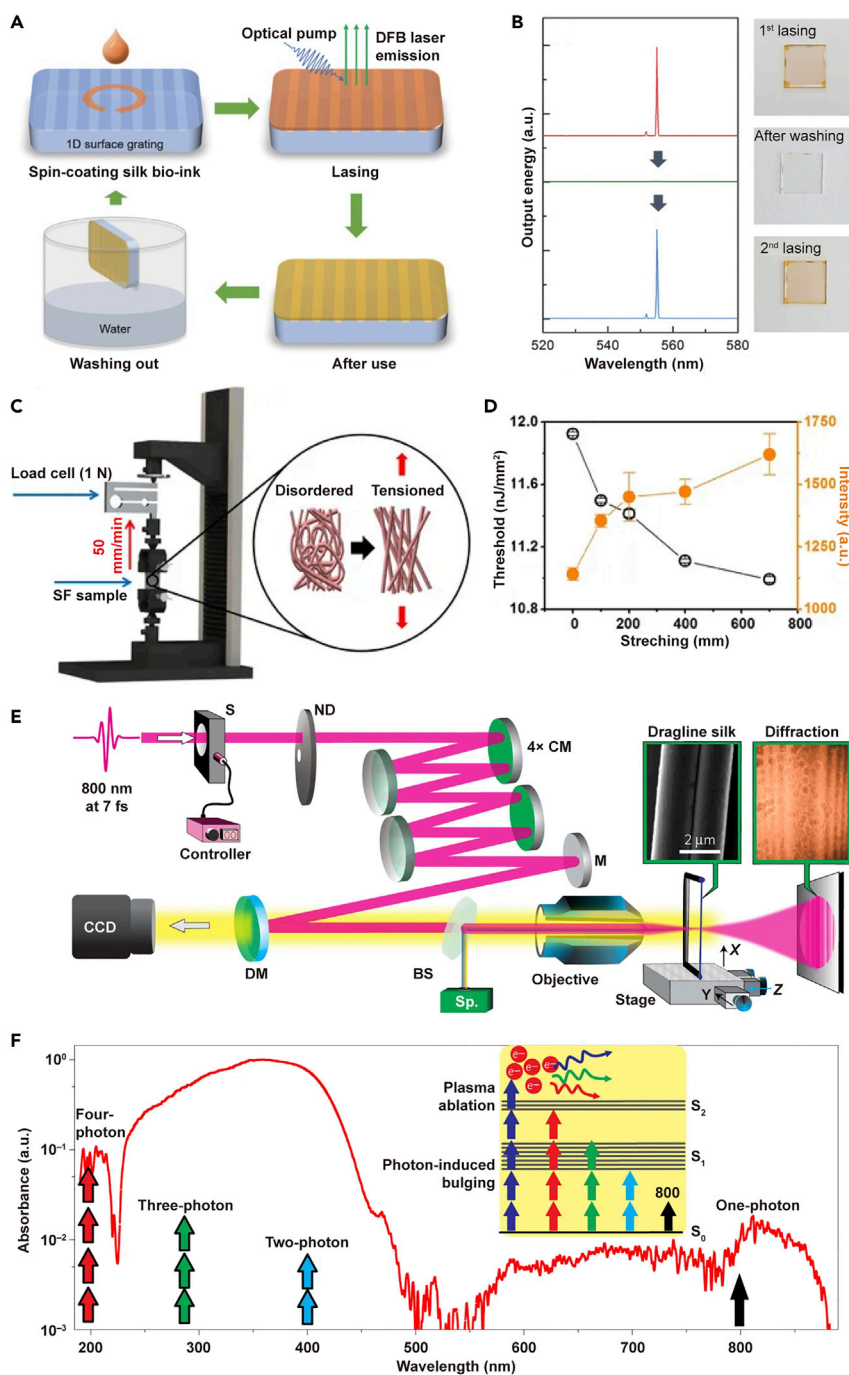


Figure 8. SF Materials in Nonlinear Optics

(A and B) (A) Schematic illustration of the working principles of the physically transient distributed feedback (DFB) laser using optically activated silk bio-ink and (B) the lasing spectra from the DFB laser. Reprinted with permission from Jung et al., 2016. Copyright 2016, John Wiley & Sons, Inc.

(C and D) (C) Schematic illustration of the experimental setup and (D) the measurement of Young's moduli of SF nanofibrous scaffolds. Reprinted with permission from Kim et al., 2017. Copyright 2017, Nature Publishing Group.

(E and F) Schematic illustration of (E) the experimental setup and (F) the mechanisms of laser-silk interaction; scale bar: 2 μm. Reprinted with permission from Sidhu et al., 2017. Copyright 2014, Nature Publishing Group.

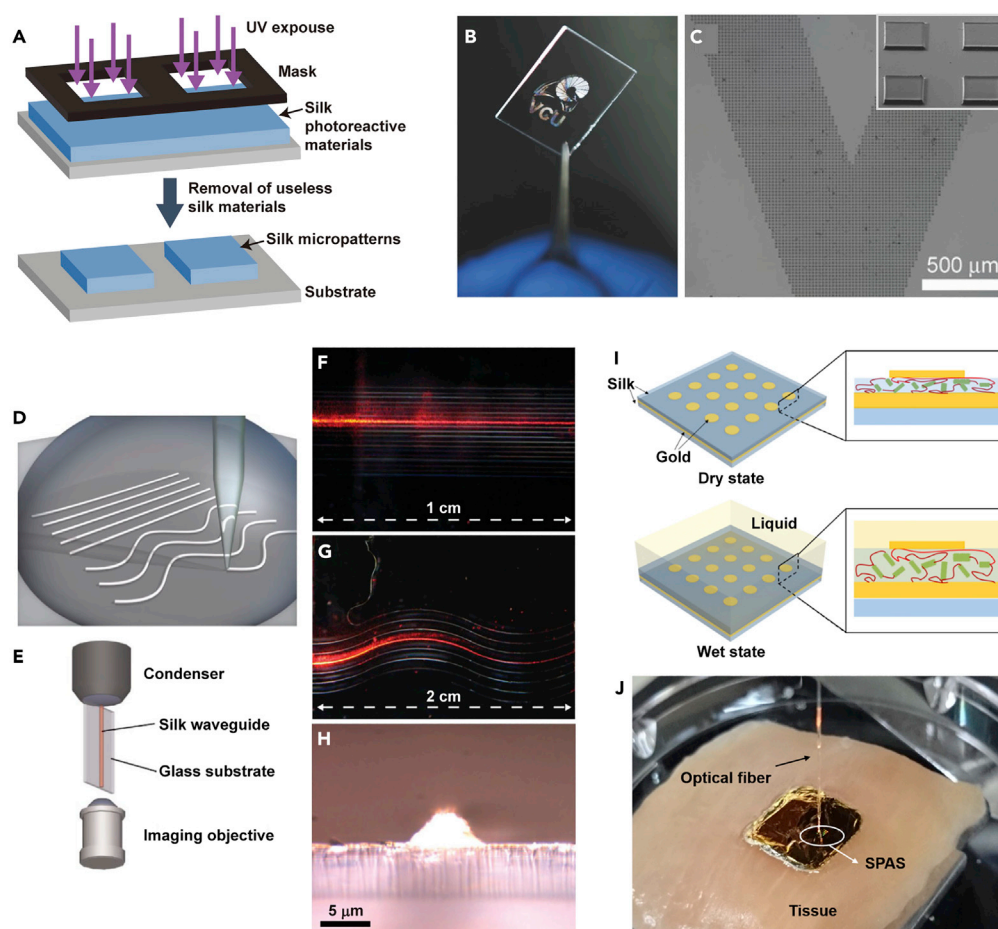


Figure 9. Optical Elements of SF Materials

(A) Schematic of the fabrication of microstructures using silk protein lithography.

(B and C) An image and scanning electron microscope (SEM) images of 10- μm squares patterned to form the "VCU logo"; scale bar: 500 μm . Reprinted with permission from Kurland et al., 2014. Copyright 2014, John Wiley & Sons, Inc. (D–H) Schematic of (D) the direct-write assembly of silk waveguides and (E) the experimental setup. Optical images of (F) straight and (G) wavy silk waveguides guiding light from a He:Ne laser source. (H) Transverse image of the output face of a silk waveguide. Reprinted with permission from Parker et al., 2009. Copyright 2009, John Wiley & Sons, Inc. Scaling bars indicate 1 cm (in F), 2 cm (in G) and 5 μm (in H), respectively.

(I and J) (I) Schematic of the working principle of the silk plasmonic absorber sensor (SPAS) and an image of an SPAS on chicken breast tissue. Reprinted with permission from Lee et al., 2015. Copyright 2015, American Chemical Society.

A set of bioactive diffractive optical elements microfabricated using functionalized SF films are applied in sensing applications, including hydration sensing, biological concealment, therapeutic treatment, and *in vitro* and *in vivo* drug-release monitoring upon degradation (Zhou et al., 2017). Naturally occurring iridescent systems produce brilliant color displays through the multiscale, hierarchical assembly of structures that combine the reflective, diffractive, diffusive, and absorbing domains. Hierarchical 3D PCs are fabricated using SF by a topographical templating strategy that combines the reflective, diffractive, diffusive, and absorbing domains. The generated 2D diffractive optics composed of 3D nanophotonic lattices allow simultaneous control over the reflection (through the 3D PBG) and transmission (through 2D diffractive structuring) of light (Wang et al., 2017, 2018).

Bio-optical Fibers of Silk Fibroin Materials

SF protein optical fibers with wave-guiding properties are fabricated for five wavelengths (473.0; 632.8; 964.0; 1,311; and 1,552 nm). Optical scattering losses are measured by the fiber probe technique at 632.8 nm and were estimated to be 0.22 dB cm^{-1} (Prajzler et al., 2018). Optical fibers were fabricated using

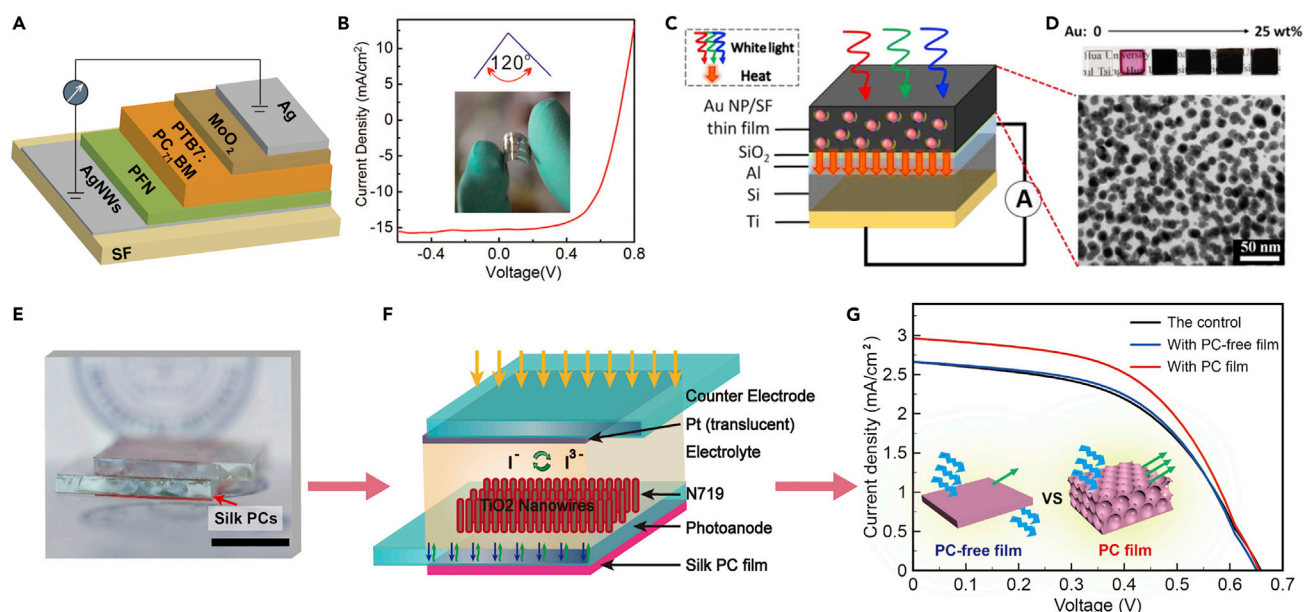


Figure 10. SF Materials in Solar Cells

(A) Schematic illustration of an organic solar cell (OSC).

(B) Current density (J)–voltage (V) curves of OSCs with a bending angle of $\sim 120^\circ$. Reprinted with permission from Liu et al., 2014. Copyright 2014, American Chemical Society.

(C and D) (C) Schematic illustration of an AuNPs/SF thin film with an attached Al/Si Schottky diode under white light; (D) images of AuNPs/SF thin films with different AuNPs contents and a cross-sectional transmission electron microscope (TEM) image of a AuNPs/SF thin film; scale bar: 50 nm. Reprinted with permission from Tsao et al., 2015. Copyright 2015, American Chemical Society.

(E–G) (E) An image and (F) schematic illustration of a DSSC with an attached fluorescent silk PC film; scale bar, 1 cm. (G) J – V curves of the DSSCs with nothing (the control), fluorescent silk PC-free film, and fluorescent silk PC film; scale bar: 1 cm. Inset: schematic of the comparison of fluorescence emission of the fluorescent silk PC-free film and the fluorescent silk PC film. Reprinted with permission from Hu et al., 2019. Copyright 2019, John Wiley & Sons, Inc.

native spider silk as raw materials and integrated into photonic chips. The optical loss of spider silk is 10.5 dB cm^{-1} , which is very promising for bio-photonics applications where light propagation and/or sensing in biocompatible media are required (Applegate et al., 2015). Silk optical waveguides with straight and wavy shapes can also be generated by direct ink writing (Figures 9D–9H). The printed silk waveguides retain their rod-like morphology by crystallizing in a methanol-rich, coagulation reservoir (Kujala et al., 2016; Parker et al., 2009). Native dragline silk was assessed in a pioneering proof-of-concept experiment, in which the optical fiber based on pristine spider silk is used as a sensor to measure humidity and chemical compounds (Qiao et al., 2017; Tow et al., 2018).

SF films hybridized with chitin nanofibres are optically transparent, and their use as a biocompatible structural platform for emerging wearable devices (e.g., contact-lens-type glucose sensors) and advanced displays (e.g., transparent plastic cover windows) has been demonstrated (Hong et al., 2018). Moreover, biocompatible silk microfilms can be used in a glucose sensor with a very high sensitivity of $1,200 \text{ nm/RIU}$ (refractive index units) and high relative intensity change (Figures 9I and 9J). The top layer of the device is a 2D gold disk array, the bottom layer is a gold mirror, and the interlayer is a silk spacer layer with a thickness of 20 nm. The silk spacer absorbs the environmental liquid, such as glucose, and consequently swells; the changed volume and refractive index of the swelled silk layer reflect the surface plasmon resonance behavior that results in the absorption of the incident wave (Lee et al., 2015).

Light Energy Conversion Devices

Solar Cells

Silk materials possess poor light stability under sunlight; thus, silk materials seem to offer no advantage over solar batteries. However, silk films exhibit high transparency, excellent lightness, biocompatibility and flexibility, and they can be subjected to large-scale roll-to-roll processing, which plays an important role in flexible and biodegradable electronics. As a very important biomaterial, silk can be processed

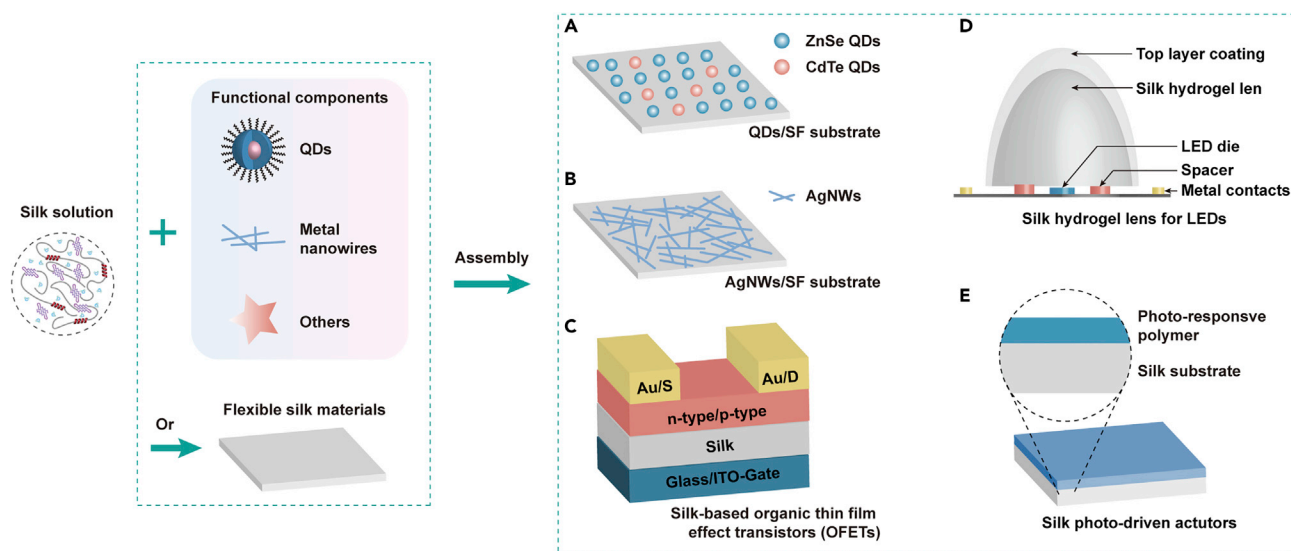


Figure 11. Silk Materials in Light-emitting Devices and Photo-driven Actuators

(A–E) Silk materials work as the structural materials in (A) QDs/SF substrate and (B) AgNWs/SF substrate, the insulator layer in (C) silk-based organic thin-film effect transistors (OFETs), the high refractive index materials in (D) silk hydrogel lens for LEDs, and the flexible substrate in (E) silk photo-driven actuators.

into flexible electronic devices for implantation and integration into the human body. A biocompatible SF substrate with a mesh of silver nanowires was fabricated into flexible organic solar cells (OSCs) (Figures 10A and 10B), achieving a conductivity of $\sim 11.0 \Omega/\text{sq}$ and transmittance of $\sim 80\%$ in the visible light range, and the conductivity remained unchanged after being bent and unbent 200 times. The maximum power conversion efficiency of OSCs reached 6.62% (Liu et al., 2014). Furthermore, SF films with gold nanoparticles exhibit white-light absorption, and when coated on a simple Al/Si Schottky diode (Figures 10C and 10D), they displayed a linear, significant, stable photo-thermo-electronic effect (Tsao et al., 2015). This photo-thermo-electronic device using gold nanoparticle-doped SF film as a source for photothermal generation has ultrahigh absorbances of approximately 95% from 350 to 750 nm and moderate absorbances ($>60\%$) at longer wavelengths (750–1000 nm) due to localized surface plasmon resonance-induced absorbance enhancement (Kojic et al., 2012). Moreover, silk material can be utilized as a mold, and bulk hetero-junction solar cells were fabricated by a simple, cost-effective nanoimprinting lithography method using a patterned SF film mold at room temperature, promoting optical absorption, interfacial area, and bicontinuous pathways (Ding et al., 2015).

Apart from as the inner component in solar cells, functionalized silk films can simply attach to commercial solar cells to increase their energy conversion efficiency (ECE). As shown in Figures 10E–10G, a fluorescent silk PC film was placed tightly against the photoanode of a backside-illuminated dye-sensitized solar cell (DSSC) to enhance the ECE (Hu et al., 2019). The hybrid fluorescent silk PC-enhanced DSSCs achieved 16% higher ECE than the control and the DSSCs with the fluorescent silk PC-free film. The improvement in ECE is attributed to the reflection of the silk PCs and the enhanced fluorescence emission. In addition, the fluorescence intensity is greatly enhanced at $\theta \approx 0^\circ$ by the silk PC self-collimator design, and the emitted light is channelled and confined to the effective collective angle to increase the ECE of the DSSCs (Kosten et al., 2013).

Light-Emitting Devices

Taking the advantage of the excellent lightness and flexibility of silk, silk-based light-emitting devices have been widely reported. For instance, QD silk films with white-light emission were prepared by controlling the molar ratio of blue luminescent ZnSe (5.2 nm) and yellow luminescent CdTe (4.1 nm) QDs (Figure 11A), resulting in a promising candidate for multicomponent light-emitting devices (Lin et al., 2014a). Silk films functionalized with Ag nanowires (AgNWs), as a type of conductive transparent substrate, were employed to fabricate flexible organic light-emitting diodes (Figure 11B), and the obtained flexible organic light-emitting diodes have a current efficiency of 19 cd A^{-1} (Liu et al., 2015). An advanced unipolar n-type organic light-emitting transistor was achieved by using SF as a thin-film dielectric in an organic thin-film structure

(Figure 11C), and the silk-based optoelectronic yields a light emission of 100 nW (Capelli et al., 2011). Furthermore, SF hydrogel has been reported as the lens in light-emitting diodes (Figure 11D), and it has a light extraction efficiency over 0.95 on a warm white-light-emitting diode (LED). The stability of the silk hydrogel lens is enhanced approximately three-fold by using a biocompatible/biodegradable poly(ester-urethane) coating and more than three orders of magnitude by using an edible paraffin wax coating (Melikov et al., 2017).

Photo-Driven Actuators

Photo-driven actuators, which are a machine component that move under light, are very promising for applications in complicated programmed artificial muscles. Rapid and reversible photo-driven actuators were fabricated with an active linear azobenzene polymer layer and a passive SF substrate (Figures 11E). In contrast to conventional oriented azobenzene liquid crystalline elastomers, this type of actuator has an unimorph structure with unique bending properties (Wen et al., 2014). The response speed of the unimorph actuator is on the level of a few hundred milliseconds, and the bending angle can be well controlled by the intensity of UV light irradiation or adjustment of the thickness of the two layers. Photo-driven actuators can also be constructed in fiber form. Silk fiber photo-driven actuators blended with photoisomerizable chromophore molecules—azobenzenebromide can convert the energy of unpolarized light directly into mechanical work with a well-defined direction of action (Krasnov et al., 2015).

Photochemical Reaction of Silk Materials

UV Resistance

The stability of silk fibers under UV light is an issue of significant concern regarding both the appearance retention of silk-derived products and the preservation of historic silk textiles. Silk cocoons can protect silkworms from various threats, including UV damage, during the pupal stage. A higher sericin content toward the outer part of the cocoon shell forms an effective shield to protect pupae from UV radiation and resists the photo-degradation of silk fibers (Kaur et al., 2013). Regarding proteomic profiling of silk photo-oxidation, silk fiber is particularly susceptible to UV-induced coloration changes because it is rich in tyrosine (5% of the total heavy chain), which (together with tryptophan and phenylalanine) is one of the key amino acids responsible for photo-induced protein discoloration because tyrosine provides many potential oxidation sites on the SF chain.

To reduce the silk photo-oxidation process, silk materials were functionalized with some UV absorbers. As the most popular method in the past, silk was weighted with tin to make up for the loss of weight after degumming. A light (pink) tin weight results in heavy oxidation due to the presence of tin(IV) oxohydroxide compounds, which act as photosensitizers that absorb UV, whereas a heavy (dynamite) tin weight leads to the formation of high levels of protein crosslinking and high UV resistance (Solazzo et al., 2012).

With the development of materials science, various UV absorbers/shelters have been investigated to protect silks from UV damage. Nanoparticles, such as TiO₂ (Gao et al., 2017), AgTiO₂ (Xiao et al., 2015), CeO₂ (Lu et al., 2014), FeSO₄ (Mongkholrattanasit et al., 2011), and TiO₂@Ag (Li et al., 2011), are assembled onto a silk substrate through covalent/noncovalent linkages that can absorb UV light to endow silk with UV-shielding ability. Silk fabrics can also be colored by gold nanoparticles that were synthesized *in situ* through induction by sunlight, resulting in high light resistance, including strong UV-blocking properties and excellent fastness to sunlight (Yao et al., 2016). Moreover, the modified silk fabric achieved a decrease in UV-visible transmittance (together with yellowing) by a covalent coupling reaction between the tyrosine residues on SF and a hydroxyphenyl benzotriazole UV absorber containing a diazonium group (Chen et al., 2015). The presence of the conjugated azo-benzotriazole chromophore leads to a very low color change and a light decrease in tensile strength compared with untreated silk fabric following UV irradiation.

Photocatalysis

As an ancient textile, silk can be directly used as a fabric or easily processed into porous materials to host nanostructured photocatalysts, such as TiO₂, ZnO, and Ag. The silk-based porous materials act as a support in the functionalization process, providing a 3D mesoscale platform for the photocatalysis of functional compounds. For example, a type of Ag@AgCl-polyurethane/SF (Ag@AgCl-PU/SF) composite porous film was synthesized through an *in situ* decoration process, exhibiting high photocatalytic activity for the degradation of rhodamine B and antibacterial activity (Zhou et al., 2019). Based on the nano-TiO₂ photocatalyst, a

silk paper respirator with dust resistance and antibacterial properties was prepared (Sha and Zhao, 2012), and the pore structure and filtration performance of the silk respirator paper could be controlled by changing the degree of beating of the silk pulp and the basis weight of the silk paper.

Light-Assisted Synthesis

Photo-crosslinking is a common method used to prepare silk hydrogels for biomedical applications. A highly elastic Rec1-resilin/SF (Rec1/SF)-based hydrogel was fabricated by a rapid photo-crosslinking reaction with the formation of dityrosine crosslinks. The Rec1-SF hybrid hydrogels combine the highly elastic soft phase of Rec1-resilin and the mechanically strong hard phase of *Bombyx mori* SF. The UV-induced crosslinking method provides a rapid route for tuning the elasticity and strength of Rec1-SF hybrid hydrogels for tissue engineering applications (Whittaker et al., 2015). Another SF hydrogel was achieved by a photochemically crosslinking reaction that used tris(2,2-bipyridyl) dichloro ruthenium(II) hexahydrate ($\text{Ru(II)(bpy)}_3^{2+}$) as the catalyst and ammonium persulphate as the electron acceptor (Whittaker et al., 2014). In addition, SF/poly(vinyl alcohol) (SF/PVA) hydrogels were photo-crosslinked and applied in the delivery of macromolecular drugs (Kundu et al., 2012).

Apart from regenerated SF materials, regenerated sericin can also be used in a light-assisted crosslinked form to produce precise protein micropatterns for use in tissue engineering and cell culture applications. Photoreactive sericin can be synthesized by solubilizing the sericin in 1-M LiCl/dimethyl sulfoxide (DMSO) solution followed by reaction with stoichiometric 2-isocyanatoethyl methacrylate at 60°C for 5 h in dry N_2 . The photoreactive sericin can be spin-coated or cast on various substrates including silicon, glass, indium tin oxide (ITO), or polydimethylsiloxane (PDMS) to form homogeneous films for photolithography (Applegate et al., 2016; Pal et al., 2016).

Moreover, silk can provide effective reaction sites for light-assisted synthesis via electrostatic absorption or ion exchange. A type of Ag nanoparticle (AgNP)-coated silk fiber was reportedly produced through an UV-assisted *in situ* synthesis for antibacterial applications. The AgNPs efficiently attached to the silk surface in an irradiation time-dependent manner and showed excellent crystalline structures (Lu et al., 2014). Light-assisted synthesis, as an environment-friendly method, is a facile, green, and cost-effective approach for the production of biocompatible functionalized silk materials, with low cell cytotoxicity.

Sensing and Imaging with Silk Fibroin Materials

Humidity Sensing Based on Silk Photonics and Cyclic Contraction

In most reported silk-based sensors, silk always works as a flexible substrate. However, here, we highlight an intrinsic humidity-responsive feature of silk materials. The so-called humidity-induced cyclic contraction property was found in animal silks (mainly spider and silkworm silk) and their regenerated derivatives. For silk PCs, changes in humidity lead to cyclic contractions of SF materials (Agnarsson et al., 2009), giving rise to variation in the lattice parameters of open spheres in the silk PCs, a. By taking advantage of this behavior, silk materials were developed as various biocompatible silk PC-based humidity sensors with high sensitivity (Figure 12A). As the reflection peaks (corresponding to the PBG) can be tuned by a, silk PC materials with visible reflection peak redshifts of 16 nm (with a sensitivity of 0.32 nm/% relative humidity [RH]) and UV peak shifts of 6 nm (with a sensitivity of 0.12 nm/% RH) occur as the humidity decreases from 80% to 30% (Figures 12B and 12C). In contrast, blueshifts occur as the humidity level increases. During the cyclic process, the shifts in the reflection peaks are also reversible, allowing precise tuning of the reflection peaks of an SF inverse opal within a certain range (Figure 12D).

Furthermore, the PBG shifts of the silk PCs give rise to the humidity responses of the fluorescence signal of silk PCs. Figure 12E shows a fluorescent silk PC sensor that produces a remarkably improved sensitivity of 28.50 a.u./% RH (80.78 times higher than that of the control), with an increased linearity of 97.08% (from 37% to 74% RH). During the cyclic process (Figure 12F), the fluorescence intensity shifts of the silk PC sensor are reversible and stable (humidity: 28%–75% RH), whereas the control displays almost no response. The silk PC-based humidity sensors show high sensitivity, rapid response, and excellent reproducibility.

Non-invasive Imaging and Biomedical Applications

Silk materials, including gels, fibers, and sponges, are suitable for use as *in vivo* implanted materials due to their biocompatibility; however, visualizing the evolution of silk materials *in vivo* has become

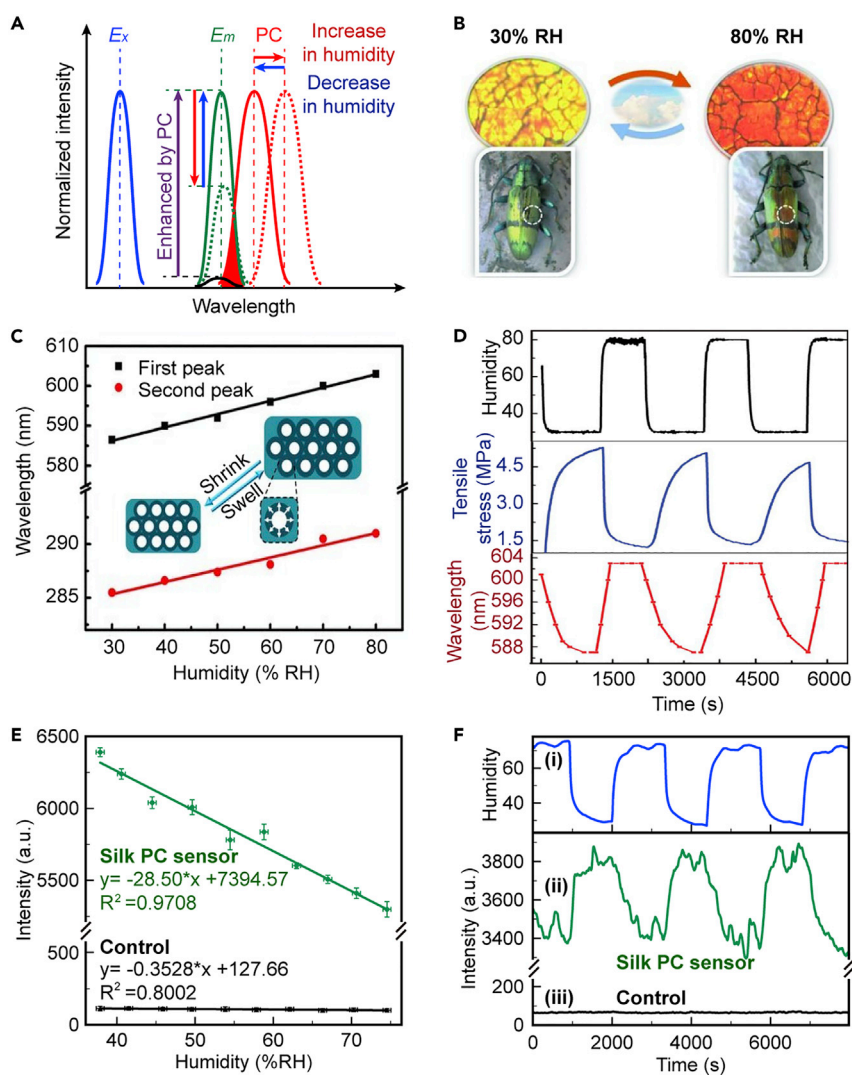


Figure 12. Silk PC-based Humidity Sensors

(A) Schematic of tuning the reflection peak and fluorescence intensity by PBG shift due to humidity changes. Reprinted with permission from Hu et al., 2019. Copyright 2019, John Wiley & Sons, Inc.

(B–D) Illustration of (B) coloration change and (C) reflection peaks shifts of silk PCs at various humidity levels. (D) Measurements of cyclic tensile stress and reflection peak of silk PCs in response to the humidity change. Reprinted with permission from Diao et al., 2013. Copyright 2013, John Wiley & Sons, Inc.

(E and F) Fluorescence emission (E) at different humidity levels and (F) with rapid changes in humidity for fluorescent silk PCs and the control. Reprinted with permission from Hu et al., 2019. Copyright 2019, John Wiley & Sons, Inc.

a major challenge (Amirikia et al., 2018). Taking the advantage of the NIR optical window (ca. 700–900 nm), NIR imaging techniques, such as one-photon, two-photon, and upconversion fluorescent techniques, are powerful tools for the non-invasive visualization of silk materials in real time in tissue and *in vivo* (Figure 13A).

One-Photon Fluorescence Imaging. As a feasible one-photon fluorescent materials, Au nanoclusters (AuNCs) have received extensive attention owing to not only their remarkable NIR fluorescence light but also their good photostability, low toxicity, high biocompatibility, and ease of synthesis. AuNCs are dispersed evenly and bound to silk bioscaffolds for bioimaging (Figures 13B and 13C), and the problems of authenticity and quality of bioimaging have been successfully overcome (Lin et al., 2016).

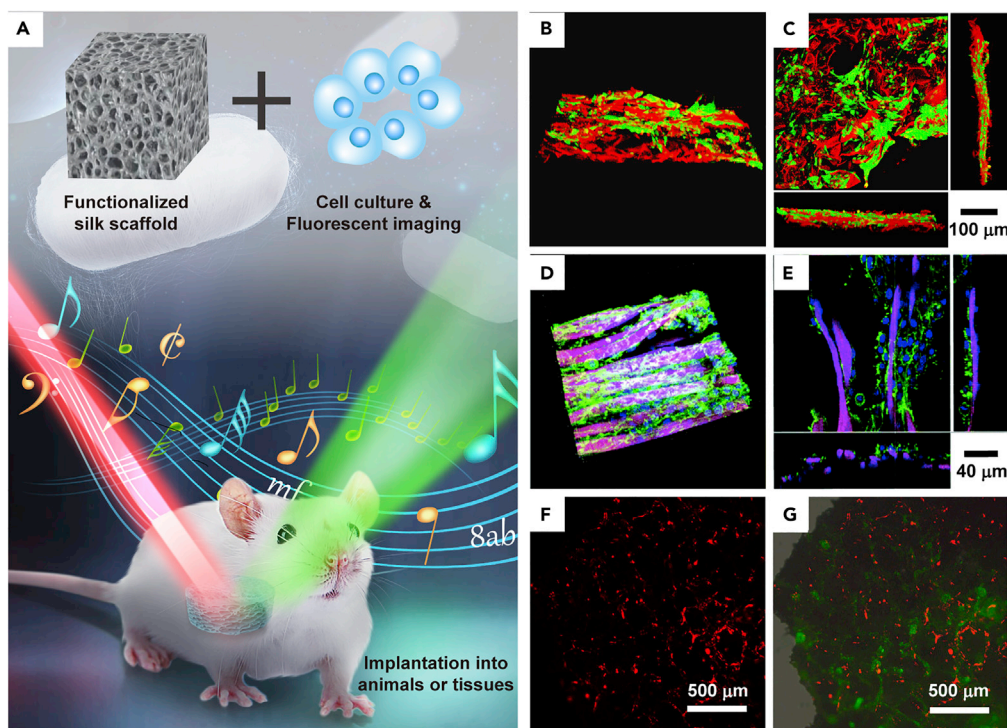


Figure 13. SF Materials in Non-invasive Biomedical Imaging Applications

(A) Illustration of the bioimaging of functionalized SF materials.

(B and C) Fluorescence confocal microscope images of AuNC-functionalized silk scaffolds (red) and osteoblast cells (green); scale bar: 100 μm . Reprinted with permission from Lin et al., 2016. Copyright 2016, John Wiley & Sons, Inc.

(D and E) TPF microscope images of the two-photon fluorescent fabric scaffolds (pink) and 3T3 fibroblast cells (blue and green); scale bar: 40 μm . Reprinted with permission from Lin et al., 2014. Copyright 2014, The Royal Society of Chemistry.

(F and G) Fluorescence microscope images of UCNP-functionalized silk scaffolds (green) and MC3T3-E1 cells (red); scale bar: 500 μm . Reprinted with permission from Song et al., 2017. Copyright 2014, John Wiley & Sons, Inc.

Two-Photon Fluorescence Imaging. Compared with one-photon fluorescence imaging using AuNCs as dyes, the two-photon fluorescence (TPF) imaging of silk scaffolds based on organic molecules and QDs is of interest in a wide variety of fields (Figures 13D and 13E), because it has several major advantages over current detection technologies, such as its intrinsic optical sectioning capability, low NIR absorption from endogenous species and water, and large penetration depth (Lin et al., 2012, 2014, 2015; Zheng et al., 2015). The greatest challenge for TPF imaging is that the light source is a femtosecond laser, which is very expensive and difficult to maintain.

Upconversion Fluorescence Imaging. In contrast, upconversion fluorescent technique, whose light source is an inexpensive and stable continuous laser, has emerged for the imaging of silk scaffolds. The assembly of lanthanide (Ln)-doped upconversion nanoparticles into silk materials was implemented to acquire upconversion fluorescent emission (Figures 13F and 13G), and functionalized silk scaffolds were implanted subcutaneously into mice, resulting in fluorescence for *in vivo* bioimaging (Song et al., 2017).

Other Fluorescence Imaging Methods. Recently, silk cocoons have been graphitized to form graphene oxide, resulting in remarkable fluorescence, multiphoton imaging, and magnetic properties. The obtained graphene oxide has a maximum excitation wavelength of 380 nm and emits 460-nm fluorescence. It also has significant two-photon absorption (TPA) at NIR wavelengths (Roy et al., 2014). Nanospheres fabricated from SF and nanodiamonds are loaded with the anthracycline doxorubicin (DoX) to study the drug-release kinetics. Nanodiamonds provide fluorescence for imaging, whereas degradable SF spheres stabilize and release the drug in a controlled manner (Khalid et al., 2016).

CONCLUSIONS AND FUTURE PERSPECTIVES

The optical properties of SF materials have been considered since ancient times. SF fibers have been used as cloth for thousands of years due to their exquisite quality, smoothness, breathability, beautiful color, and bright luster. Currently, the optical transparency of SF films and the dyeability and fluorescence of SF fibers have been widely and deeply studied by modern techniques, such as reactive dyeing, transgenosis, MMA, and biomimetics. Silk materials have a wide range of applications, including optical elements, nonlinear optics, light energy conversion, UV resistance, photocatalysis, UV-assisted synthesis, sensing, and bioimaging.

Silks are impressive biomaterials that can interact with light. Nevertheless, certain questions, especially concerning light and mechanical stability and cost, are still unanswered. As we know, optical biomaterials, such as fluorescent-labeled polypeptides or genes and photothermal and photochemical reaction biomaterials, are biomaterials that can undergo physical or chemical changes when exposed to light. In recent years, optical biomaterials have attracted extensive attention for biosensor imaging and drug delivery applications. We can foresee a great demand to produce silk materials with optical functions, including luminescence, stimuli sensitivity, and photovoltaic and photocatalytic properties, for applications in biophotonics, bioelectronics, biomedicine, etc. We hope that this review not only summarizes the importance and development of the optical properties of silk materials but also inspires researchers to design and create novel optical properties based on a better understanding of the interaction between light and silk materials.

ACKNOWLEDGMENTS

This work was financially supported by 111 project (B16029), the National Natural Science Foundation of China (51773171, 21705135), the Doctoral Fund of the Ministry of Education (20130121110018), the Science and Technology Project of Xiamen City (3502Z20183012), the Science and Technology Planning Project of Guangdong Province (2018B030331001), the Fujian Provincial Department of Science and Technology (2017J06019), the Shenzhen Science and Technology Plan Project (JCYJ20180504170208402), and the 1000 Talents Program of Xiamen University. The authors are also thankful for technical support from Drs. Likun Yang, Hao Wang, Rui Yu, and Yun Yang.

AUTHOR CONTRIBUTIONS

All authors (F.H., N.B.L., and X.Y.L.) jointly conceptualized the paper and contributed to the original and revised drafts.

REFERENCES

- Agnarsson, I., Dhinojwala, A., Sahni, V., and Blackledge, T.A. (2009). Spider silk as a novel high performance biomimetic muscle driven by humidity. *J. Exp. Biol.* 212, 1990–1994.
- Agrawal, A. (1999). Glow-in-the-dark silk. *Nat. Biotechnol.* 17, 412.
- Amirikia, M., Shariatzadeh, S.M.A., Jorsaraei, S.G.A., and Mehranjani, M.S. (2018). Auto-fluorescence of a silk fibroin-based scaffold and its interference with fluorophores in labeled cells. *Eur. Biophys. J. Biophys.* 47, 573–581.
- Amsden, J.J., Domachuk, P., Gopinath, A., White, R.D., Negro, L.D., Kaplan, D.L., and Omenetto, F.G. (2010). Rapid nanoimprinting of silk fibroin films for biophotonic applications. *Adv. Mater.* 22, 1746–1749.
- Applegate, M.B., Marelli, B., Kaplan, D.L., and Omenetto, F.G. (2013). Determination of multiphoton absorption of silk fibroin using the Z-scan technique. *Opt. Express* 21, 29637–29642.
- Applegate, M.B., Perotto, G., Kaplan, D.L., and Omenetto, F.G. (2015). Biocompatible silk step-index optical waveguides. *Biomed. Opt. Express* 6, 4221–4227.
- Applegate, M.B., Partlow, B.P., Coburn, J., Marelli, B., Pirie, C., Pineda, R., Kaplan, D.L., and Omenetto, F.G. (2016). Photocrosslinking of silk fibroin using riboflavin for ocular prostheses. *Adv. Mater.* 28, 2417–2420.
- Bucciarelli, A., Mulloni, V., Maniglio, D., Pal, R.K., Yadavalli, V.K., Motta, A., and Quaranta, A. (2018). A comparative study of the refractive index of silk protein thin films towards biomaterial based optical devices. *Opt. Mater.* 78, 407–414.
- Capelli, R., Amsden, J.J., Generali, G., Toffanin, S., Benfenati, V., Muccini, M., Kaplan, D.L., Omenetto, F.G., and Zamboni, R. (2011). Integration of silk protein in organic and light-emitting transistors. *Org. Electron.* 12, 1146–1151.
- Cavallini, S., Toffanin, S., Chieco, C., Sagnella, A., Formaggio, F., Pistone, A., Posati, T., Natali, M., Caprini, M., Benfenati, V., et al. (2015). Naturally functionalized silk as useful material for photonic applications. *Compos. B Eng.* 71, 152–158.
- Chen, W., Wang, Z., Cui, Z., Pan, D., and Millington, K. (2015). Improving the photostability of silk using a covalently-bound UV absorber. *Polym. Degrad. Stab.* 121, 187–192.
- Choi, S.H., Kim, S.W., Ku, Z., Visbal-Onufrak, M.A., Kim, S.R., Choi, K.H., Ko, H., Choi, W., Urbas, A.M., Goo, T.W., et al. (2018). Anderson light localization in biological nanostructures of native silk. *Nat. Commun.* 9, 452.
- Chu, M.Q., and Liu, G.J. (2008). Fluorescent silkworm silk prepared via incorporation of green, yellow, red, and near-infrared fluorescent quantum dots. *IEEE T. Nanotechnol.* 7, 308–315.
- Cohen-Karni, T., Jeong, K.J., Tsui, J.H., Reznor, G., Mustata, M., Wanunu, M., Graham, A., Marks, C., Bell, D.C., Langer, R., et al. (2012). Nanocomposite gold–silk nanofibers. *Nano Lett.* 12, 5403–5406.
- da Silva, R.R., Cavicchioli, M., Lima, L.R., Otoni, C.G., Barud, H.S., Santagnelli, S.H., Tercjak, A., Amaral, A.C., Carvalho, R.A., and Ribeiro, S.J.L. (2017). Fabrication of biocompatible, functional, and transparent hybrid films based on silk fibroin

and epoxy silane for biophotonics. *ACS Appl. Mater. Interfaces* 9, 27905–27917.

Daimon, T., Hirayama, C., Kanai, M., Ruike, Y., Meng, Y., Kosegawa, E., Nakamura, M., Tsujimoto, G., Katsuma, S., and Shimada, T. (2010). The silkworm *Green b* locus encodes a quercetin 5-O-glucosyltransferase that produces green cocoons with UV-shielding properties. *Proc. Natl. Acad. Sci. U S A* 107, 11471–11476.

Diao, Y.Y., Liu, X.Y., Toh, G.W., Shi, L., and Zi, J. (2013). Multiple structural coloring of silk-fibroin photonic crystals and humidity-responsive color sensing. *Adv. Funct. Mater.* 23, 5373–5380.

Ding, G., Jin, Q., Chen, Q., Hu, Z., and Liu, J. (2015). The fabrication of ordered bulk heterojunction solar cell by nanoimprinting lithography method using patterned silk fibroin mold at room temperature. *Nanoscale Res. Lett.* 10, 491.

Gao, S., Huang, J., Li, S., Liu, H., Li, F., Li, Y., Chen, G., and Lai, Y. (2017). Facile construction of robust fluorine-free superhydrophobic TiO₂@fabrics with excellent anti-fouling, water-oil separation and UV-protective properties. *Mater. Des.* 128, 1–8.

Honda, R., Ryu, M., Li, J.-L., Mizeikis, V., Juodkazis, S., and Morikawa, J. (2018). Simple multi-wavelength imaging of birefringence: case study of silk. *Sci. Rep.* 8, 17652.

Hong, M.S., Choi, G.M., Kim, J., Jang, J., Choi, B., Kim, J.K., Jeong, S., Leem, S., Kwon, H.Y., Hwang, H.B., et al. (2018). Biomimetic chitin-silk hybrids: an optically transparent structural platform for wearable devices and advanced electronics. *Adv. Funct. Mater.* 28, 1705480.

Hu, F., Liu, W., Li, W., Xu, Z., Diao, Y.Y., Lin, N., Guo, W., Shi, L., van Esch, J.H., and Liu, X.Y. (2019). Silk fluorescence collimator for ultrasensitive humidity sensing and light-harvesting in semitransparent dye-sensitized solar cells. *Small* 15, 1804171.

Hu, X., Xue, R., Cao, G., Zhang, X., Zhang, Y., Yu, X., Zhang, Y., and Gong, C. (2012). Elementary research of the formation mechanism of sex-related fluorescent cocoon of silkworm, *Bombyx mori*. *Mol. Biol. Rep.* 39, 1395–1409.

Iizuka, T., Sezutsu, H., Tatematsu, K., Kobayashi, I., Yonemura, N., Uchino, K., Nakajima, K., Kojima, K., Takabayashi, C., Machii, H., et al. (2013). Colored fluorescent silk made by transgenic silkworms. *Adv. Funct. Mater.* 23, 5232–5239.

Jung, H., Min, K., Jeon, H., and Kim, S. (2016). Physically transient distributed feedback laser using optically activated silk bio-ink. *Adv. Opt. Mater.* 4, 1738–1743.

Kaur, J., Rajkhowa, R., Tsuzuki, T., Millington, K., Zhang, J., and Wang, X. (2013). Photoprotection by silk cocoons. *Biomacromolecules* 14, 3660–3667.

Khalid, A., Mitropoulos, A.N., Marelli, B., Tomljenovic-Hanic, S., and Omenetto, F.G. (2016). Doxorubicin loaded nanodiamond-silk spheres for fluorescence tracking and controlled drug release. *Biomed. Opt. Express* 7, 132–147.

Kharlampieva, E., Kozlovskaya, V., Gunawidjaja, R., Shevchenko, V.V., Vaia, R., Naik, R.R., Kaplan,

D.L., and Tsukruk, V.V. (2010). Flexible silk-inorganic nanocomposites: from transparent to highly reflective. *Adv. Funct. Mater.* 20, 840–846.

Kim, Y., and Choi, J. (2015). Dyeing properties of microbial prodiginine from *Zooshikella rubidus* for silk fabrics. *Fibers Polym.* 16, 1981–1987.

Kim, S., Yang, S., Choi, S.H., Kim, Y.L., Ryu, W., and Joo, C. (2017). Random lasing from structurally-modulated silk fibroin nanofibers. *Sci. Rep.* 7, 4506.

Kojic, N., Pritchard, E.M., Tao, H., Brenckle, M.A., Mondia, J.P., Panilaitis, B., Omenetto, F., and Kaplan, D.L. (2012). Focal infection treatment using laser-mediated heating of injectable silk hydrogels with gold nanoparticles. *Adv. Funct. Mater.* 22, 3793–3798.

Kosten, E.D., Atwater, J.H., Parsons, J., Polman, A., and Atwater, H.A. (2013). Highly efficient GaAs solar cells by limiting light emission angle. *Light Sci. Appl.* 2, e45.

Krasnov, I., Krekienė, N.R., Krywka, C., Jung, U., Zillohu, A.U., Strunskus, T., Elbahri, M., Magnussen, O.M., and Mueller, M. (2015). Optically switchable natural silk. *Appl. Phys. Lett.* 106, 093702.

Kujala, S., Mannila, A., Karvonen, L., Kieu, K., and Sun, Z. (2016). Natural silk as a photonics component: a study on its light guiding and nonlinear optical properties. *Sci. Rep.* 6, 22358.

Kundu, J., Poole-Warren, L.A., Martens, P., and Kundu, S.C. (2012). Silk fibroin/poly(vinyl alcohol) photocrosslinked hydrogels for delivery of macromolecular drugs. *Acta Biomater.* 8, 1720–1729.

Kurland, N.E., Dey, T., Wang, C., Kundu, S.C., and Yadavalli, V.K. (2014). Silk protein lithography as a route to fabricate sericin microarchitectures. *Adv. Mater.* 26, 4431–4437.

Lee, M., Jeon, H., and Kim, S. (2015). A highly tunable and fully biocompatible silk nanoplasmonic optical sensor. *Nano Lett.* 15, 3358–3363.

Lee, B., Kwon, H., Kim, S., and Rotermund, F. (2016). Natural silk protein as a new broadband nonlinear optical material. *Opt. Mater. Express* 6, 993–1002.

Li, Z., Jiang, Y., Cao, G., Li, J., Xue, R., and Gong, C. (2015). Construction of transgenic silkworm spinning antibacterial silk with fluorescence. *Mol. Biol. Rep.* 42, 19–25.

Lin, N., Liu, X.Y., Diao, Y.Y., Xu, H., Chen, C., Ouyang, X., Yang, H., and Ji, W. (2012). Switching on fluorescence emission by molecular recognition and aggregation dissociation. *Adv. Funct. Mater.* 22, 361–368.

Lin, N., Hu, F., Sun, Y., Wu, C., Xu, H., and Liu, X.Y. (2014a). Construction of white-light-emitting silk protein hybrid films by molecular recognized assembly among hierarchical structures. *Adv. Funct. Mater.* 24, 5284–5290.

Lin, N., Meng, Z., Toh, G.W., Zhen, Y., Diao, Y., Xu, H., and Liu, X.Y. (2015). Engineering of fluorescent emission of silk fibroin composite materials by material assembly. *Small* 11, 1205–1214.

Li, G.H., Liu, H., Zhao, H.S., Gao, Y.Q., Wang, J.Y., Jiang, H.D., and Boughton, R.I. (2011). Chemical assembly of TiO₂ and TiO₂@Ag nanoparticles on silk fiber to produce multifunctional fabrics. *J. Colloid Interfaces Sci.* 358, 307–315.

Lin, N., Cao, L., Huang, Q., Wang, C., Wang, Y., Zhou, J., and Liu, X.-Y. (2016). Functionalization of silk fibroin materials at mesoscale. *Adv. Funct. Mater.* 26, 8885–8902.

Lin, N., Toh, G.W., Feng, Y., Liu, X.Y., and Xu, H. (2014). Two-photon fluorescent *Bombyx mori* silk by molecular recognition functionalization. *J. Mater. Chem. B* 2, 2136–2143.

Ling, S., Li, C., Jin, K., Kaplan, D.L., and Buehler, M.J. (2016). Liquid exfoliated natural silk nanofibrils: applications in optical and electrical devices. *Adv. Mater.* 28, 7783–7790.

Liu, Y., Qi, N., Song, T., Jia, M., Xia, Z., Yuan, Z., Yuan, W., Zhang, K.Q., and Sun, B. (2014). Highly flexible and lightweight organic solar cells on biocompatible silk fibroin. *ACS Appl. Mater. Interfaces* 6, 20670–20675.

Liu, Y., Xie, Y., Liu, Y., Song, T., Zhang, K.Q., Liao, L., and Sun, B. (2015). Flexible organic light emitting diodes fabricated on biocompatible silk fibroin substrate. *Semicond. Sci. Technol.* 30, 104004.

Lu, Z., Mao, C., Meng, M., Liu, S., Tian, Y., Yu, L., Sun, B., and Li, C.M. (2014). Fabrication of CeO₂ nanoparticle-modified silk for UV protection and antibacterial applications. *J. Colloid Interfaces Sci.* 435, 8–14.

Lu, Z., Meng, M., Jiang, Y., and Xie, J. (2014). UV-assisted *in situ* synthesis of silver nanoparticles on silk fibers for antibacterial applications. *Colloids Surf. A* 447, 1–7.

MacLeod, J., and Rosei, F. (2013). Sustainable sensors from silk. *Nat. Mater.* 12, 98–100.

Madhukumar, R., Asha, S., Rao, B.L., Sarojini, B.K., Byrappa, K., Wang, Y., and Sangappa, Y. (2015). Optical properties of gamma-irradiated *Bombyx mori* silk fibroin films. *Radiat. Eff. Defects Sol.* 170, 906–915.

Melikov, R., Press, D.A., Kumar, B.G., Dogru, I.B., Sadeghi, S., Chirea, M., Yilgor, I., and Nizamoglu, S. (2017). Silk-hydrogel lenses for light-emitting diodes. *Sci. Rep.* 7, 7258.

Mondia, J.P., Amsden, J.J., Lin, D., Dal Negro, L., Kaplan, D.L., and Omenetto, F.G. (2010). Rapid nanoimprinting of doped silk films for enhanced fluorescence emission. *Adv. Mater.* 22, 4596–4599.

Mongkhrolrattanasit, R., Krystufek, J., Wiener, J., and Vikova, S. (2011). UV protection properties of silk fabric dyed with eucalyptus leaf extract. *J. Textile I* 102, 272–279.

Neo, P.Y., Tan, D.J.A., Shi, P., Toh, S.L., and Goh, J.C.-H. (2015). Enhancing analysis of cells and proteins by fluorescence imaging on silk-based biomaterials: modulating the autofluorescence of silk. *Tissue Eng. Part C Methods* 21, 218–228.

Nisal, A., Trivedy, K., Mohammad, H., Panneri, S., Sen Gupta, S., Lele, A., Manchala, R., Kumar, N.S., Gadgil, M., Khandewal, H., et al. (2014). Uptake of azo dyes into silk glands for production of colored

- silk cocoons using a green feeding approach. *ACS Sustain. Chem. Eng.* **2**, 312–317.
- Pal, R.K., Farghaly, A.A., Collinson, M.M., Kundu, S.C., and Yadavalli, V.K. (2016). Photolithographic micropatterning of conducting polymers on flexible silk matrices. *Adv. Mater.* **28**, 1406–1412.
- Palermo, G., Barberi, L., Perotto, G., Caputo, R., De Sio, L., Umeton, C., and Omenetto, F.G. (2017). Conformal silk-azobenzene composite for optically switchable diffractive structures. *ACS Appl. Mater. Interfaces* **9**, 30951–30957.
- Parekh, N.M., and Maheria, K.C. (2014). Colorimetric studies of heterocyclic monoazo reactive dyes and their dyeing applications on cotton, silk, and wool fibers. *Res. Chem. Intermed.* **40**, 1003–1019.
- Parker, S.T., Domachuk, P., Amsden, J., Bressner, J., Lewis, J.A., Kaplan, D.L., and Omenetto, F.G. (2009). Biocompatible silk printed optical waveguides. *Adv. Mater.* **21**, 2411–2415.
- Perotto, G., Cittadini, M., Tao, H., Kim, S., Yang, M., Kaplan, D.L., Martucci, A., and Omenetto, F.G. (2015). Fabrication of tunable, high-refractive-index titanate-silk nanocomposites on the micro- and nanoscale. *Adv. Mater.* **27**, 6728–6732.
- Perotto, G., Zhang, Y., Naskar, D., Patel, N., Kaplan, D.L., Kundu, S.C., and Omenetto, F.G. (2017). The optical properties of regenerated silk fibroin films obtained from different sources. *Appl. Phys. Lett.* **111**, 103702.
- Perry, H., Gopinath, A., Kaplan, D.L., Dal Negro, L., and Omenetto, F.G. (2008). Nano- and micropatterning of optically transparent, mechanically robust, biocompatible silk fibroin films. *Adv. Mater.* **20**, 3070–3072.
- Place, E.S., Evans, N.D., and Stevens, M.M. (2009). Complexity in biomaterials for tissue engineering. *Nat. Mater.* **8**, 457–470.
- Prabhu, K.H., Teli, M.D., and Waghmare, N.G. (2011). Eco-friendly dyeing using natural mordant extracted from *Emblica officinalis* G. Fruit on cotton and silk fabrics with antibacterial activity. *Fibers Polym.* **12**, 753–759.
- Prajzler, V., Min, K., Kim, S., and Nekvindova, P. (2018). The investigation of the waveguiding properties of silk fibroin from the visible to near-infrared spectrum. *Materials* **11**, 112.
- Pugina, R.S., da Rocha, E.G., Ribeiro, S.J.L., and Caiu, J.M.A. (2019). Study of the energy transfer process in rare earth-doped silk fibroin for future application in luminescent compounds. *J. Lumin.* **205**, 423–428.
- Punrattanasin, N., Nakpathom, M., Somboon, B., Narumol, N., Rungruangkitkrai, N., and Mongkholrattanasit, R. (2013). Silk fabric dyeing with natural dye from mangrove bark (*Rhizophora apiculata Blume*) extract. *Ind. Crops Prod.* **49**, 122–129.
- Qiao, X., Qian, Z., Li, J., Sun, H., Han, Y., Xia, X., Zhou, J., Wang, C., Wang, Y., and Wang, C. (2017). Synthetic engineering of spider silk fiber as implantable optical waveguides for low-loss light guiding. *ACS Appl. Mater. Interfaces* **9**, 14665–14676.
- Roy, M., Kusrkar, T.S., Maurya, S.K., Meena, S.K., Singh, S.K., Sethy, N., Bhargava, K., Sharma, R.K., Goswami, D., Sarkar, S., et al. (2014). Graphene oxide from silk cocoon: a novel magnetic fluorophore for multi-photon imaging. *3 Biotech.* **4**, 67–75.
- Service, R.F. (2008). Coming soon to a knee near you: cartilage like your very own. *Science* **322**, 1460–1461.
- Sha, L., and Zhao, H. (2012). Preparation and properties of nano-TiO₂ photo-catalytic silk respirator paper. *Fibers Polym.* **13**, 1159–1164.
- Shimanovich, U., Pinotsi, D., Shimanovich, K., Yu, N., Bolisetty, S., Adamcik, J., Mezzenga, R., Charmet, J., Vollrath, F., Gazit, E., et al. (2018). Biophotonics of native silk fibrils. *Macromol. Biosci.* **18**, 1700295.
- Sidhu, M.S., Kumar, B., and Singh, K.P. (2017). The processing and heterostructuring of silk with light. *Nat. Mater.* **16**, 938–945.
- Solazzo, C., Dyer, J.M., Deb-Choudhury, S., Clerens, S., and Wyeth, P. (2012). Proteomic profiling of the photo-oxidation of silk fibroin: implications for historic tin-weighted silk. *Photochem. Photobiol.* **88**, 1217–1226.
- Song, Y., Lin, Z., Kong, L., Xing, Y., Lin, N., Zhang, Z., Chen, B.-H., and Liu, X.Y. (2017). Meso-functionalization of silk fibroin by upconversion fluorescence and near infrared *in vivo* biosensing. *Adv. Funct. Mater.* **27**, 1700628.
- Tansil, N.C., Li, Y., Teng, C.P., Zhang, S., Win, K.Y., Chen, X., Liu, X.Y., and Han, M.Y. (2011). Intrinsically colored and luminescent silk. *Adv. Mater.* **23**, 1463–1466.
- Toffanin, S., Kim, S., Cavallini, S., Natali, M., Benfenati, V., Amsden, J.J., Kaplan, D.L., Zamboni, R., Muccini, M., and Omenetto, F.G. (2012). Low-threshold blue lasing from silk fibroin thin films. *Appl. Phys. Lett.* **101**, 091110.
- Tow, K.H., Chow, D.M., Vollrath, F., Dicaire, I., Gheysens, T., and Thevenaz, L. (2018). Exploring the use of native spider silk as an optical fiber for chemical sensing. *J. Lightwave Technol.* **36**, 1138–1144.
- Tsao, S.H., Wan, D., Lai, Y.S., Chang, H.M., Yu, C.C., Lin, K.T., and Chen, H.L. (2015). White-light-induced collective heating of gold nanocomposite/*Bombyx mori* silk thin films with ultrahigh broadband absorbance. *ACS Nano* **9**, 12045–12059.
- Vepari, C., and Kaplan, D.L. (2007). Silk as a biomaterial. *Prog. Polym. Sci.* **32**, 991–1007.
- Wang, Y., Aurelio, D., Li, W., Tseng, P., Zheng, Z., Li, M., Kaplan, D.L., Liscidini, M., and Omenetto, F.G. (2017). Modulation of multiscale 3D lattices through conformational control: painting silk inverse opals with water and light. *Adv. Mater.* **29**, 1702769.
- Wang, Y., Li, W., Li, M., Zhao, S., De Ferrari, F., Liscidini, M., and Omenetto, F.G. (2018). Biomaterial-based "structured opals" with programmable combination of diffractive optical elements and photonic bandgap effects. *Adv. Mater.* **31**, e1805312.
- Wen, H., Zhang, W., Weng, Y., and Hu, Z. (2014). Photomechanical bending of linear azobenzene polymer. *RSC Adv.* **4**, 11776–11781.
- Whittaker, J.L., Choudhury, N.R., Dutta, N.K., and Zannettino, A. (2014). Facile and rapid ruthenium mediated photo-crosslinking of *Bombyx mori* silk fibroin. *J. Mater. Chem. B* **2**, 6259–6270.
- Whittaker, J.L., Dutta, N.K., Elvin, C.M., and Choudhury, N.R. (2015). Fabrication of highly elastic resilin/silk fibroin based hydrogel by rapid photo-crosslinking reaction. *J. Mater. Chem. B* **3**, 6576–6579.
- Xiao, X., Liu, X., Chen, F., Fang, D., Zhang, C., Xia, L., and Xu, W. (2015). Highly anti-UV properties of silk fiber with uniform and conformal nanoscale TiO₂ coatings via atomic layer deposition. *ACS Appl. Mater. Interfaces* **7**, 21326–21333.
- Yao, Y., Tang, B., Chen, W., Sun, L., and Wang, X. (2016). Sunlight-induced coloration of silk. *Nanoscale Res. Lett.* **11**, 1–9.
- Zhang, P., Lan, J., Wang, Y., Xiong, Z.H., and Huang, C.Z. (2015). Luminescent golden silk and fabric through *in situ* chemically coating pristine-silk with gold nanoclusters. *Biomaterials* **36**, 26–32.
- Zhang, F., Zhao, Y., Chen, X., Xu, A.Y., Huang, J.T., and Lu, C.D. (1999). Fluorescent transgenic silkworm. *Acta Biochem. Biophys. Sin.* **31**, 119–123.
- Zhao, Y., Hien, K.T.T., Mizutani, G., and Rutt, H.N. (2017). Second-order nonlinear optical microscopy of spider silk. *Appl. Phys. B* **123**, 188.
- Zheng, Z.Z., Liu, M., Guo, S.Z., Wu, J.B., Lu, D.S., Li, G., Liu, S.S., Wang, X.Q., and Kaplan, D.L. (2015). Incorporation of quantum dots into silk biomaterials for fluorescence imaging. *J. Mater. Chem. B* **3**, 6509–6519.
- Zhou, Z., Shi, Z., Cai, X., Zhang, S., Corder, S.G., Li, X., Zhang, Y., Zhang, G., Chen, L., Liu, M., et al. (2017). The use of functionalized silk fibroin films as a platform for optical diffraction-based sensing applications. *Adv. Mater.* **29**, 1605471.
- Zhou, H., Wang, X., Wang, T., Zeng, J., Yuan, Z., Jian, J., Zhou, Z., Zeng, L., and Yang, H. (2019). *In situ* decoration of Ag@AgCl nanoparticles on polyurethane/silk fibroin composite porous films for photocatalytic and antibacterial applications. *Eur. Polym. J.* **118**, 153–162.